

High-resolution wall-to-wall land-cover mapping and land change assessment for Australia from 1985 to 2015



Marco Calderón-Loor^{a,b,*}, Michalis Hadjikakou^a, Brett A. Bryan^a

^a Centre for Integrative Ecology, School of Life and Environmental Sciences, Deakin University, Melbourne, Australia

^b Grupo de Investigación de Biodiversidad, Medio Ambiente y Salud—BIOMAS, Universidad de las Américas (UDLA), Quito, Ecuador

ARTICLE INFO

Keywords:

Land-cover change
Landsat
Random Forest
Google earth engine
Ground-truth data

ABSTRACT

Computational and data handling limitations have constrained time-series analyses of land-cover change at high-spatial resolution over large (e.g., continental) extents. However, a new set of cloud-computing services offer an opportunity for improving knowledge of land change at finer grain. We constructed a historical set of seven high-resolution wall-to-wall land-cover maps at continental scale for Australia and analyzed temporal and spatial changes of land-cover from 1985 to 2015 at 5-year time-steps using Google Earth Engine (GEE). We used 281,962 Landsat scenes for producing median cloud-free composites at each time-step. We established a pseudo ground-truth dataset and used a PCA-based outlier detection method to reduce its uncertainty. A random forest model was trained at each time-step for classifying raw data into six land-cover classes: Cropland, Forest, Grassland, Built-up, Water, and Other areas, using 49 predictor datasets and nearly 20,000 training points. We further constructed uncertainty maps at each time-step as a proxy of per-pixel confidence. The average overall accuracy of the seven 30 m-resolution land-cover maps was ~93%. Built-up and Water areas displayed the highest user and producer accuracies (>93%), with Grasslands and Other areas slightly lower (~82–88%). Classification uncertainty was lower in more homogeneous landscapes (i.e., large expanses of a single land-cover class). Around 510,975 km² ($\pm 69,877 \text{ km}^2$) of land changed over the 30 years at an average of $\sim 17,033 \text{ km}^2 \text{ yr}^{-1}$ ($\pm 2329 \text{ km}^2 \text{ yr}^{-1}$). Cropland and Forests declined by $\sim 64,836 \text{ km}^2$ ($\pm 16,437 \text{ km}^2$) and $\sim 152,492 \text{ km}^2$ ($\pm 24,749 \text{ km}^2$) over 30 years, mainly converting to Grassland. Built-up areas experienced the highest relative increases, increasing from 12,320 km² in 1985 to 15,013 km² in 2015 ($\sim 19.2\%, \pm 3.1\%$). The sensitivity, i.e., proportion of pixels correctly classified as having changed, was over 96%, whereas the specificity, i.e., the proportion of pixels correctly classified as no-change, was over 68%. Numerous potential applications of these first-of-their-kind, detailed spatiotemporal maps of land use and land-change assessment exist spanning many areas of environmental impact assessment, policy, and management. Similarly, this methodological framework can provide a useful template for assessing continental-scale, high-resolution land dynamics more broadly.

1. Introduction

Land cover has a significant influence on ecosystem function at all spatial scales, from global to local (e.g. Bonan, 2008; Marques et al., 2019; Peters et al., 2019; Song et al., 2018). Changes in human population, climatic conditions (IPCC, 2014), agri-food demand (Alexander et al., 2016a), and a range of other socioeconomic and biophysical factors (Popp et al., 2017) determine the pace and direction of land-use and land-cover change (hereafter simply *land change*) (Hurt et al., 2011). Land change monitoring has become a critically important task for assessing both the effect of global change on land, and the impact of

land change on ecosystem services, biogeochemical dynamics, and natural habitat and species diversity, and sustainability more broadly (Foley et al., 2005; Güneralp et al., 2013; Song et al., 2018; Turner et al., 2007). Although historical land change information at a national level is available at coarse spatial resolution (e.g., $\geq 100\text{-m}$) (Bontemps et al., 2013; Lymburner et al., 2011), knowledge of land change at high spatial resolution over larger national and continental areas remains limited (Alexander et al., 2016b; Congalton et al., 2014; van Vliet et al., 2016).

Land change assessment relies mainly on the availability of classified spatial information, usually supported by ancillary variables (Hasegawa et al., 2017; Heck et al., 2018; Verburg et al., 2015). There are numerous

* Corresponding author at: Centre for Integrative Ecology, School of Life and Environmental Sciences, Deakin University, Melbourne, Australia.

E-mail addresses: mcalderonloor@deakin.edu.au (M. Calderón-Loor), m.hadjikakou@deakin.edu.au (M. Hadjikakou), b.bryan@deakin.edu.au (B.A. Bryan).

existing coarse-resolution global land-cover products including the 1-km resolution IGBP DISCover (Loveland et al., 2000) and UMD Land Cover (Hansen et al., 2000) datasets; the 300-m resolution GLOBCOVER (Arino et al., 2007), Corine Land Cover (Bossard et al., 2000), and ESA CCI Land Cover (Bontemps et al., 2013) layers, and; the 250-m resolution MODIS Land Cover dataset (Friedl et al., 2010). However, their intrinsic uncertainties added to their spatial and thematic resolution, make them unfit for local environmental and land change assessments occurring at a finer resolution than the cell size of the land-cover maps (Giri et al., 2013; Townshend et al., 2012; Verburg et al., 2004; Wulder et al., 2008). For instance, Seto et al. (2011) underscored the need for classified high spatial resolution imagery for accurately identifying urban growth and attributed the source of the large variations in future urban area (ranging from 430,000 km² to 12,500,000 km² for 2030) to variation in estimates of current urban extent produced with coarse spatial imagery (Potere and Schneider, 2007).

Advances in land change monitoring are occurring rapidly in response to the increasing availability of high and medium-resolution satellite imagery (MacLachlan et al., 2017; Young et al., 2017) and to the emergence of cloud-computing services (Xiong et al., 2017). New high-resolution global land-cover products are being released at 30-m (Chen et al., 2015) and 10-m resolution (Gong et al., 2019). However, challenges still exist. The scarcity of historical ground-truth data and the high computational costs for producing them have limited the production of consistent high-resolution land-cover maps over large areas. For instance, around 10,000 Landsat scenes (~3 terabytes of data) are required for representing global land-cover at a single time slice (Giri et al., 2013). The emergence of proprietary web-based platforms such as Google Earth Engine (GEE; <https://earthengine.google.com>) (Gorelick et al., 2017) are drastically reducing the computation times and expanding the potential for analyzing big geospatial data. GEE contains a growing catalogue of geospatial data and satellite imagery from different sources and sensors that can be analyzed and stored, reducing data processing and storage requirements. While a growing body of research is exploiting the capabilities of GEE for different purposes (e.g. Hansen et al., 2013; Koskinen et al., 2019; Wang et al., 2019), land-cover mapping over large extents is still limited. Only three continental-scale studies have made use of the platform's built-in algorithms for producing multiclass, time-series land-cover classification, focusing on Africa (Midekisa et al., 2017), Brazil (MapBiomas, 2019), and Central Asia (Hu and Hu, 2019).

The classification of raw spatial imagery is commonly performed by employing supervised classification methods (Brown et al., 2013; Tan et al., 2013; Townshend et al., 2012). Supervised methods assign a label to a cell by comparing the similarity of the features of each pixel to a training dataset (Ali et al., 2016; Hansen et al., 2000; Wang et al., 2019). Among supervised methods, machine learning classifiers have been shown to outperform classic parametric algorithms for classification of large dimensional and complex landscapes (Denisko and Hoffman, 2018; Reichstein et al., 2019; Rodriguez-Galiano et al., 2012; Wang et al., 2019). However, classification accuracy depends not only in the classifier but also on the training and validation datasets (Carlotto, 2009; Pelletier et al., 2017) which can significantly affect estimates of land change over time (Pontius Jr and Li, 2010). Because collecting ground-truth training data can be resource consuming, a range of sources (e.g., optical imagery, aerial photos, crowd sourcing, cadastral and government data) are regularly used for building *pseudo* training/validation datasets. Errors arising from differing land-cover class definition, low spatial resolution and classification accuracy of reference data, differing time of data collection, and the prevalence of spectrally-similar classes among other factors, can influence the quality of the pseudo ground-truth dataset and reduce classification accuracy (Foody, 2002; Foody and Mathur, 2006; Pelletier et al., 2017). While robust-to-noise machine learning classifiers have the added advantage of being relatively insensitive to low levels of noise in the training dataset (i.e., <20%) (Rodriguez-Galiano et al., 2012), a quality assurance check of

pseudo ground-truth data quality is recommended—although rarely employed—when levels of noise are >20%, or when noise levels are unknown (Mellor et al., 2015; Na et al., 2009).

Australia—the focus of our study—is a country with a heterogeneous landscape and complex land change processes. Major transformations in the Australian landscape began after European settlement, driven by “... [An] unrestricted access to land, technological change and growth in productivity and population” (Lesslie and Mewett, 2018). High rates of agricultural expansion, urban growth and land clearance have resulted from increases in population size and structure, economic growth, improvement in transport access, trade agreements, and innovation in technology (Grundy et al., 2016; Lesslie, 2011; Seabrook et al., 2006). New land-uses on the Australian landscape such as mining activities, forestry and carbon farming, and nature conservation add a layer of complexity to current and future land change (Bryan et al., 2016). Currently, consistent national land-cover data is available at 250-m resolution from 2001 onwards at an annual time-step (Lymburner et al., 2011). However, the limited resolution, time-series, and lack of per-pixel accuracy information hampers the assessment of long-term land change dynamics at a national scale (Alexander et al., 2016b; Güneralp and Seto, 2013; Prestele et al., 2016; van Vliet et al., 2016). Hence, a robust framework for increasing the spatial resolution, extending the historical time-series, and reducing the uncertainty of continental land-cover and land change mapping in Australia and more broadly is required to underpin a better understanding of key land system processes (Hoskins et al., 2016) and the complex patterns (Klotz et al., 2016) involved in local land change.

Here, we present the first consistent, high-resolution, long time-series, wall-to-wall analysis of land-cover and land change for Australia. Using a combination of cloud-based (i.e., GEE) and local computational workflow, we mapped land-cover at 30-m resolution across the entire Australian continent at five-yearly time-steps from 1985 to 2015 by analyzing 281,962 Landsat scenes. The main objectives of this work were to: (i) develop a consistent set of historical land-cover and uncertainty maps at high-spatial resolution for an extended time period covering significant changes to the Australian landscape; (ii) identify land-cover change patterns at national and local scale; and, (iii) assess the accuracy of the land-cover and land change mapping over large areas. Because no historical ground-truth data are available for Australia, we used the Dynamic Land Cover Dataset v2.1 (DLCD) (Lymburner et al., 2011) to guide our pseudo ground-truth reference dataset. Using a PCA-based outlier detection method we reduced the uncertainty in the training and validation datasets and used them to classify the raw satellite imagery at each time-step using a random forest (RF) classifier. The resulting maps include six broad land-cover classes: Cropland, Forest, Grassland, Built-up, Water, and Other. We quantified the accuracy and uncertainty of our classification and summarized land-cover change at national and local scales. We discuss the socio-economic and environmental implications of the land change assessment for Australia and the potential of the methodological innovation for land change assessment of other nations.

2. Methods

2.1. Study area

The focus of this study is continental Australia, with an area of 7,688,287 km², comprising 89 bioregions and 419 subregions (Thackway and Cresswell, 1995). Land-cover and land-use information for the country is available at coarse resolution. The DLCD v2.1 is produced at a yearly time-step at 250-m resolution using MODIS imagery from 2001 onwards, and maps Australia's land-cover into 22 classes (Lymburner et al., 2011). Land-use information is produced under the Australian Collaborative Land Use and Management Program (ACLUMP) using the Australian Land Use and Management (ALUM) classification system (ABARES, 2016). ALUM maps are produced at two scales—national

(1,250,000) and catchment scale (resolutions range from 1:5000 to 1:250,000)—using a combination of coarse resolution satellite imagery, agricultural census, and secondary data (Lesslie and Mewett, 2018). Other mapping efforts include the fractional ground cover monitoring at 500-m (Guerschman et al., 2009) that are also available for the monitoring of specific land changes, which also combines coarse spatial imagery and census information. Although the process employed for producing these maps is well documented, spatially-explicit information of their accuracy is absent.

2.2. Land-cover classification

Our wall-to-wall land-cover classification for Australia combined cloud-based and local computing approaches to pre-process, classify, validate, post-process, and analyze land-cover and land change (Fig. 1). We mapped land-cover from 1985 to 2015 at 5-year time steps at a grid cell resolution of 30-m. Each map consists of ~8.5 billion pixels. Despite its spatial resolution, we used the DLCD as reference information because of its internal consistency, its thematic resolution, and its territory-specific land-cover classes. We defined 6 broad land-cover classes for our classification (Table 1). The reference dataset (see Section 2.2.2) was produced by aggregating the 22 DLCD land-cover classes into these 6 classes (Table S1). We based this choice considering the constraints that the broad spectral resolution of the Landsat sensors (Thematic Mapper (TM), Enhanced Thematic Mapper (ETM+), and

Table 1
Land-cover classes and definitions used in this study.

Land-cover class	Definition
Cropland	Irrigated and rainfed cropping area (annual and permanent).
Forest	Tree-dominated areas with at least 20% canopy cover and a potential to reach over 2 m in height (National Forest Inventory, 1998). Includes: closed, open, sparse and scattered trees.
Grassland	Irrigated and rainfed managed and native pastures, chenopods, tussock and hummock grasses (Ali et al., 2016).
Built-up	Artificial surfaces inside urban centres and their buffer areas.
Water	Permanent inland water bodies.
Other areas	Land-cover classes that differ, spectrally or by definition, from the rest of the classes. Includes: bare lands, mines, wetlands and salt lakes.

Operation Land Imager (OLI)) impose when used for classifying spectrally similar land-cover classes (Young et al., 2017).

2.2.1. Landsat data and other predictor variables

We used 281,962 atmospherically-corrected Landsat scenes to map land-cover including Landsat 5 (123,299 scenes), Landsat 7 (120,134 scenes), and Landsat 8 (38,529 scenes). At each time-step (i.e., 1985, 1990, 1995, 2000, 2005, 2010, 2015), we created a stack of images for the target year \pm two years (e.g., images from 1998 to 2002 were used for producing the year 2000 mosaic), for minimizing missing data and

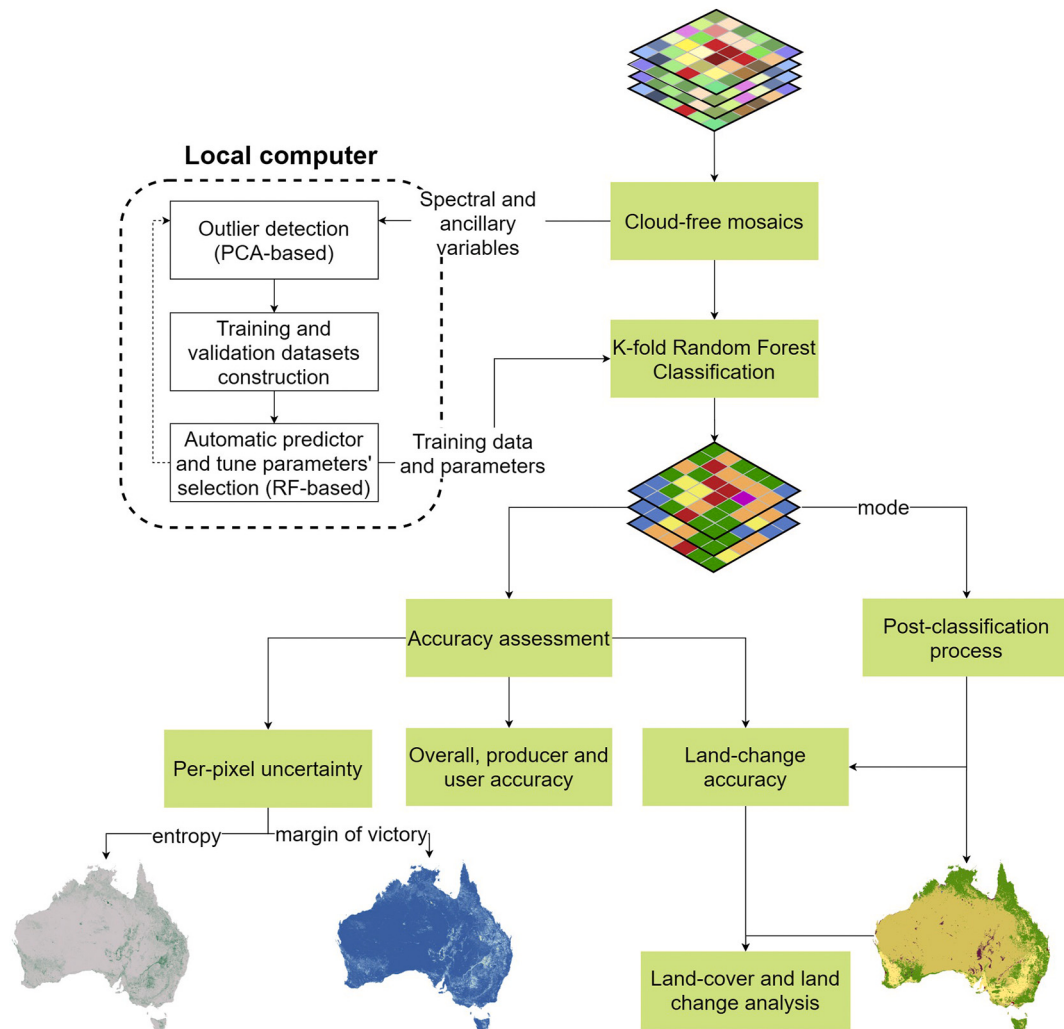


Fig. 1. Methodological approach for land-cover classification. Processes highlighted in green were performed in Google Earth Engine. (For interpretation of the references to colour in this figure legend, the reader is referred to the web version of this article.)

cloud interference (Scarth et al., 2015). We then applied the FMASK algorithm implemented in GEE (Gorelick et al., 2017) for masking clouds, cloud-shadows and snow to every stack. Each multiyear stack contained from around 5 to 200 valid observations at pixel-level (year and location dependent, see supplementary material, Table S2). Different spectral indices were calculated and appended to the cloud-free stacks along with the spectral bands and other ancillary biophysical and bioclimatic information (resampled to 30-m resolution if necessary) for use in land-cover classification. The final composites were

produced by computing the median value of every variable at pixel-level. The data was also aggregated at different temporal resolutions for capturing seasonal variability (Table 2).

2.2.2. Pseudo ground-truth data

We used an interactive, semi-automated process for constructing a pseudo-ground truth training and validation dataset. First, we digitally sampled a total of 150,000 pixels via stratified (strata = DLCD land-cover class) random sampling. Pixels were scattered across Australia

Table 2

Ancillary variables included in the yearly composites. Dots represent the temporal aggregation of the variables tested for the land-cover classification. Variables highlighted in grey were used as final predictors in the land-cover classification process.

Predictors	Formula	Temporal aggregation												Period
		Y	D	M	J	S	F	S	J	A	O	S	N	
		F	M	A	M	J	J	S	A	S	S	S	N	
Spectral bands														
Blue ¹		•	•	•	•	•	•	•	•	•	•	•	•	1984–2017
Green ¹		•	•	•	•	•	•	•	•	•	•	•	•	1984–2017
Red ¹		•	•	•	•	•	•	•	•	•	•	•	•	1984–2017
Near Infrared (NIR) ¹		•	•	•	•	•	•	•	•	•	•	•	•	1984–2017
Short-wave Infrared 1 (SWIR 1) ¹		•	•	•	•	•	•	•	•	•	•	•	•	1984–2017
SWIR 2 ¹		•	•	•	•	•	•	•	•	•	•	•	•	1984–2017
Spectral indices														
Normalized Difference Vegetation Index ²	$\frac{NIR-Red}{NIR+Red}$ (1)	•	•	•	•	•	•	•	•	•	•	•	•	1984–2017
Enhanced Vegetation Index ³	$2.5 \times \frac{NIR-Red}{NIR+6\times Red-7.5\times Blue+1}$ (2)	•	•	•	•	•	•	•	•	•	•	•	•	1984–2017
Water Band Index ⁴	$\frac{Blue}{NIR}$ (3)	•	•	•	•	•	•	•	•	•	•	•	•	1984–2017
Normalized Difference Water Index ⁵	$\frac{Green-NIR}{Green+NIR}$ (4)	•	•	•	•	•	•	•	•	•	•	•	•	1984–2017
Modified Soil-adjusted Vegetation Index ⁶	$\frac{2\times NIR+1-\sqrt{(2\times NIR+1)^2-8\times (NIR-RED)}}{2}$ (5)	•	•	•	•	•	•	•	•	•	•	•	•	1984–2017
Soil-adjusted Vegetation Index ⁷	$1.5 \times \frac{NIR-Red}{NIR+Red+0.5}$ (6)	•	•	•	•	•	•	•	•	•	•	•	•	1984–2017
Optimized Soil-adjusted Vegetation Index ⁸	$\frac{NIR-Red}{NIR+Red+0.16}$ (7)	•	•	•	•	•	•	•	•	•	•	•	•	1984–2017
Soil-Adjusted Total Vegetation Index ⁹	$1.5 \times \frac{SWIR1-Red}{SWIR1+Red+0.5} - \frac{SWIR2}{2}$ (8)	•	•	•	•	•	•	•	•	•	•	•	•	1984–2017
Bare Soil Index ¹⁰	$\frac{(SWIR_2+Red)-(NIR+Blue)}{(SWIR_2+Red)+(NIR+Blue)}$ (9)	•	•	•	•	•	•	•	•	•	•	•	•	1984–2017
Normalized Difference Built-up Index ¹¹	$\frac{SWIR-NIR}{SWIR+NIR}$ (10)	•	•	•	•	•	•	•	•	•	•	•	•	1984–2017
Blue-Red ¹²	Blue – Red (11)	•	•	•	•	•	•	•	•	•	•	•	•	1992–2000
Blue-Green ¹²	Blue – Green (12)	•	•	•	•	•	•	•	•	•	•	•	•	1992–2000
Night-time Stable Lights (DMSP) ¹³		•												1984–2017
Normalized Difference Urban Index ¹⁴	$\frac{DMSP-NDVI}{DMSP+NDVI}$ (13)	•												1984–2017
Biophysical & bioclimatic														
Mean Annual Temperature ¹⁵												Constant		1960–1991
Annual Precipitation ¹⁵												Constant		
Elevation ¹⁶												Constant		NA
Slope												Constant		
Ecoregion ¹⁷												Constant		

Where: Y: Year; DJF: December, January and February; MAM: March, April and May; JJA: June, July and August; SON: September, October and December; FS: First semester; SS: Second Semester. Sources: ¹ Landsat 5, 7 and 8. USGS; ² Carlson and Ripley (1997); ³ Huete et al. (1997); ⁴ Peñuelas et al. (1993); ⁵ McFeeters (1996); ⁶ Qi et al. (1994); ⁷ Huete (1988); ⁸ Rondeaux et al. (1996); ⁹ Marsett et al. (2006); ¹⁰ Diek et al. (2017); ¹¹ Zha et al. (2003); ¹² Murray et al. (2018); ¹³ DMSP-OSI; ¹⁴ Huang et al. (2014); Zhang et al. (2015); ¹⁵ Hijmans et al. (2004); ¹⁶ Farr et al. (2007); ¹⁷ Olson et al. (2001).

covering all the six land-cover classes. We used the raster package ([Hijmans and van Etten, 2016](#)) in R ([Team, 2013](#)) for the stratified sampling process. Using the pixels' geographic coordinates, we downloaded to a local computer their spectral and ancillary information ([Table 2](#)) at 30-m resolution at every time-step (see 2.2.1) from GEE. Then, we labelled every pixel, at each time-step, using the year 2000 land-cover classification from the DLCD (resampled at 30-m resolution) as reference.

Due to the spatial resolution of the DLCD, the reference year and its intrinsic uncertainties, overall accuracy = 82%, we employed an outlier detection method based on the spectral characteristics (at 30-m resolution) for eliminating potentially mislabelled pixels from the pseudo-ground truth dataset. We used Principal Component Analysis (PCA) ([Wold et al., 1987](#)) for producing a low-dimensional ordination space where spectrally-similar pixels were grouped together and unrelated pixels were distant from each other. A PCA was produced for each land-cover class and time-step, using the pixel's bands and ancillary variables. Other approaches have been used for the automation of the labelling and selection of training samples ([Heremans et al., 2011; Huang et al., 2015; Zhu et al., 2016](#)), creating pseudo-invariant training points ([Vidal-Macua et al., 2017](#)) or training a classifier with limited labelled data ([Gong et al., 2019](#)). However, these methods have been only applied to local scales, a limited number of land-cover classes, or only a few time-steps. As the main objective of this process was removing dubious and mislabelled pixels, we established thresholds (visually selected) based on the scores for PC1 and PC2 of every ordination analysis. We excluded all pixels with PC1 and PC2 scores < the 20th percentile and > the 80th, i.e., pixels that were ordinated far from the centre of the cluster. [Gong et al. \(2019\)](#) tested the effect of reducing the training size in land-cover classifications at global scale and showed that a reduction up to 60% of the original training sample size caused only a 1% reduction in the overall accuracy of the land-cover classification. Although the reduction in accuracy might be higher in studies with lower training samples sizes and with different local environmental characteristics, this reference value suggests that stable classifications are possible in contexts of limited information at large-scales. The resulting seven pseudo ground truth datasets at 30-m resolution (one at each time-step) were compared and the pixels with invariant land cover over all seven time steps were retained. As the outlier process did not consider the spatial location of the pixels a final interactive visual correction was performed by hand using Google Earth Pro® for removing any remaining mislabelled points, thereby ensuring a homogenous geographical coverage and including training pixels in complex landscapes ([Nguyen and Henebry, 2019](#)). The final dataset with 28,730 points ([Table 3](#)) was divided into a training (19,552 points) and validation dataset (9178 points).

2.2.3. Supervised classification

We used a random forest (RF) classifier ([Breiman, 2001](#)) to classify land-cover. RF is a computationally efficient tree-based classifier that is robust to random and systematic label noise ([Denisko and Hoffman, 2018; Pelletier et al., 2017](#)). RF builds a number of trees n in an iterative way from random samples of the training data. The ensemble of the predictions of all trees constitutes the final model. We set the number of trees to 100; other values for n were also tested with similar results.

Table 3

Training and validation points for every class used for land-cover classification.

Class	Training	Validation
Cropland	5055	2184
Forest	4661	2447
Grassland	3864	1287
Built-up	3900	2142
Water	1568	903
Other-areas	504	215
Total	19,552	9178

We tested, on a local computer, hundreds of different combinations of ancillary variables as predictors. After running a RF model for every subset of variables (size and bands were randomly selected) in the training dataset, we selected the most parsimonious model, i.e., the model with fewest variables (to avoid computational limits in GEE) and the highest observed accuracy as measured against the validation dataset. We used the caret ([Kuhn, 2012](#)) and randomForest ([Liaw and Wiener, 2002](#)) packages in R for tuning the RF model. Seven RF models were developed in the land-cover classification process in GEE, one per time-step, with 49 variables as predictors (see [Table 2](#)). The number of variables per split (mtry) was equal to the square root of the number predictors (i.e., mtry = 7).

To avoid overfitting and to increase the robustness of our classification we used the mode of ten different RF classifications as the most-likely land-cover classification for every pixel and every time-step. Based on the k-fold cross-validation method used for assessing the uncertainty of a model estimation ([Bengio and Grandvalet, 2004](#)), we divided our training dataset into ten folds. For each fold, we performed a land-cover classification using only 80% of the training data (note that the validation dataset was not subsampled as it was only used to validate the final ensemble of the independent classifications), following a stratified random design (strata = land-cover class). The mode of the ten-independent classifications was used as the most-likely land-cover class for every pixel at each time-step. Each fold took approximately two days to run, hence the number of folds was constrained to ten to avoid exceeding computation time and memory limits in GEE.

2.2.4. Post-classification

Approximately 6^7 land-cover change combinations are possible in our study period, some less likely than others, which difficult the establishment of a robust set of transition rules for ensuring the temporal consistency of the classifications. Hence, we decided to take a transparent approach and minimise the amount of postprocessing, but also providing the user with the ability to implement their own post-processing. Only one post-classification process was implemented where all pixels classified as Built-up areas outside of urban centres defined by the 'Urban Centre and Localities' ([Australian Bureau of Statistics, 2016](#)) layer were reclassified as Other. These maps present a transparent land-cover classification and, in combination with the two per-pixel confidence layers (see [Section 2.3](#)), can be further post-processed and refined according to user preferences. Land-cover transitions and land change was calculated after this post-classification correction (see [Section 2.3](#)).

2.3. Accuracy assessment and land-cover change analysis

Using the validation dataset we calculated seven confusion matrices (one per epoch) for determining the overall, producer, and user accuracy (OA, PA, and UA, respectively) of land-cover classifications, after the Built-up area correction ([Olofsson et al., 2014](#)). We also included the omission (OE = 100-PA) and commission errors (CE = 100-UA) with every error matrix for inspecting biases in the land-cover classification ([Olofsson et al., 2013](#)). Furthermore, using the results of the ten independent land-cover classifications we calculated two per-pixel confidence metrics at each time-step for quantifying the level of agreement among the independent runs as a proxy of per-pixel confidence ([Brown et al., 2009; Shadman Roodposhti et al., 2019a](#)). The first metric is the per-pixel entropy ([Shannon, 1948](#)) (Eq. 14) that summarizes the membership and frequencies of all the land-cover classes than can be assigned to a specific pixel ([Khatami et al., 2017](#)).

$$H = - \sum_{i=0}^{n-1} [P_i \times \log_2 P_i] \quad (14)$$

Where H represents the entropy, n the number of independent classifications and P_i the probability of a given land-cover class. We established three levels of entropy: low, medium, and high when a pixel was mapped

as the same land-cover in at least seven, five, and three cases, respectively. The second per-pixel confidence measure was the margin of victory, defined as the difference between the two most common land-cover classes among the ten runs (McIver and Friedl, 2001). The margin of victory provides information not clearly represented by the entropy. For instance, a pixel classified five times as land-cover 1 and five times as land-cover 2 will have a relatively low entropy, masking its true uncertainty, but a margin of victory of zero.

For assessing the accuracy of land-cover change represented by our maps, we conducted a random validation of 1800 pixels in six sites with diverse landscape mosaics, as suggested by Foody (2010). The first site (Fig. 2A) located in Western Australia depicts a heterogeneous landscape dominated by Built-up, Forest, and Cropland areas. A large patch of Forest located in the Northern Territory dominates the second site (Fig. 2B). The third site is located in the center of Australia depicting a Built-up area surrounded mostly by Grassland (Fig. 2C). A mosaic of Forest and Grassland mainly dominates the fourth site, located in Queensland (Fig. 2D). The fifth site was located at the southeast part of Australia in Victoria where Built-up areas and Grassland dominate the landscape (Fig. 2E). The sixth site located in Tasmania comprises a mosaic of Forest, Grassland, and Built-up areas (Fig. 2F).

In every site, we visually checked the land-cover classification of 300 pixels, sampled in a stratified random approach, and the land-cover transitions (if any) across the years. We used Google Earth Pro® for assessing the temporal dynamics of every pixel. We then built binary confusion matrices for assessing whether land change or the lack of it had been correctly identified. Following Foody (2010), we calculated the: 1) sensitivity (S_1), that is the proportion of pixels correctly classified as having changed (Eq. 15); 2) specificity (S_2), that is the proportion of pixels correctly classified as having not changed (Eq. 16); and, 3) prevalence (θ), that is the proportion of pixels that changed in the period of comparison (Eq. 17) (Table 4).

Post-classification land change assessment between two time-points can often lead to erroneous estimations of change (Olofsson et al., 2014). Therefore, an error-adjustment of the area experiencing change is needed for avoiding any bias in the estimation. Following Olofsson et al. (2014) and Olofsson et al. (2013) we used information from Table 4 for determining the error-adjusted area of change and its 95% confidence intervals at the national level for every land-cover class for the period 1985–2015. We assumed the same confidence intervals for all time-steps

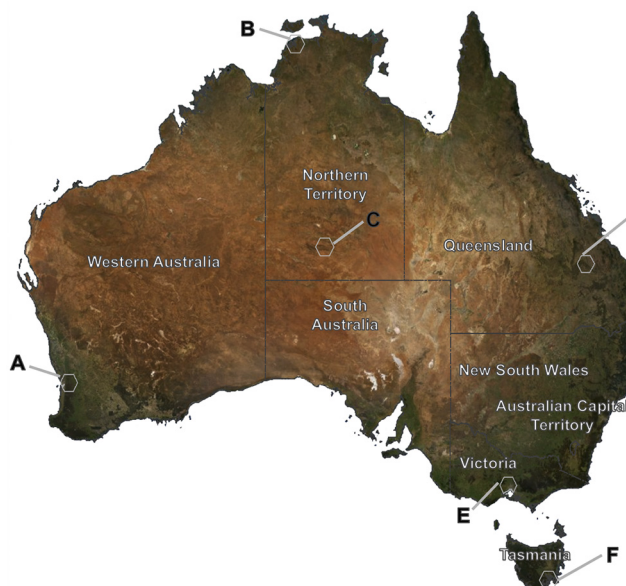


Fig. 2. Location of the six sites used to assess the accuracy of land-cover change. Background map source: DigitalGlobe ©. (1 column width).

Table 4

Binary confusion matrix for estimating the accuracy of land-cover change classification in terms of sensitivity (S_1), specificity (S_2) and prevalence (θ). Modified from (Foody, 2010).

Land-cover classification	Ground truth			$S_1 = \frac{a}{e}$ (15)
	Change	No-change	Total	
Change	a	b	g	$S_1 = \frac{a}{e}$ (15)
No-change	c	d	h	$S_2 = \frac{d}{f}$ (16)
Total	e	f	n	$\theta = \frac{e}{n}$ (17)

for each land-cover.

3. Results

3.1. Land-cover classification

A consistent time-series of seven high spatial resolution land-cover maps was created for Australia for the period 1985–2015 at five year time steps (Fig. 3). The dominant land-cover class was Grassland covering 66.3% of Australia, followed by Forest (22.9%), Cropland (8.3%), Other (2.1%), and Built-up and Water (0.2% each). Land-cover mapping had an overall accuracy of 93–94% and a user and producer accuracy from 91 to 93% over the entire study period. The 28 GB dataset is freely available for download at <https://code.earthengine.google.com/1524441de2a07f6199fdf0274870b206>. The full code used is freely available at https://github.com/mioash/lc_cover_australia.

At a land-cover class level, accuracies were more variable. For instance, the producer accuracy for 2000 varied from 86.2% to 98.6% for Grasslands and Built-up, respectively, whereas the user accuracy varied from 82.1% to 99.4% for Grasslands and Water, respectively. The same pattern was found for other years, with Grasslands and Other areas having the lowest user and PA (>82%) (see supplementary materials, Table S3). Conversely, Water and Built-up areas had the highest accuracies across all years (>93%) (Table 5). Misclassification most commonly occurred between Croplands, Forests and Grasslands.

Fig. 4 presents the entropy (Fig. 4A) and the margin of victory (Fig. 4B) of the land-cover classification for 2015. Higher levels of agreement among the classifications i.e., low entropy and high margin of victory (>60%) were present in large areas of homogeneous land-cover that remained stable over time. Conversely, areas with spatially complex landscapes tended to present medium to high entropy and low margin of victory i.e., the classifier assigned different land-cover classes to the same pixel in the individual classifications (Fig. 5). At the land-cover class level, higher uncertainty was present in areas of salt lakes, with confusion between Water, Built-up, and Other), barren-lands (confusion between Built-up and Other), and open forests and sparse vegetation (confusion between Grasslands and Forests).

3.2. Land-cover change

Land-cover transitions over the period of study showed that approximately 6.7% ($\pm 0.9\%$) of the total Australian territory experienced definitive land-cover change. Built-up areas experienced the highest relative increase of 19.2% ($\pm 3.1\%$) by 2015 compared to its extent in 1985, expanding mainly into former Grasslands ($\sim 2125 \text{ km}^2$) (Table 6). Conversely, Cropland areas suffered the highest relative loss in area of -8.6% ($\pm 2.2\%$) from 1985 to 2015. Forests also declined in area over the period of analysis of -7.8% ($\pm 1.3\%$), with the majority of these areas being converted into Grassland and Cropland. Grassland was the most stable land-cover class, with gains of 0.8% ($\pm 2.2\%$) from 1985 to 2015. The 14.8% ($\pm 4.7\%$) transitioned from Other areas, mainly into Grasslands, and the increases in Water may have resulted from misclassification.

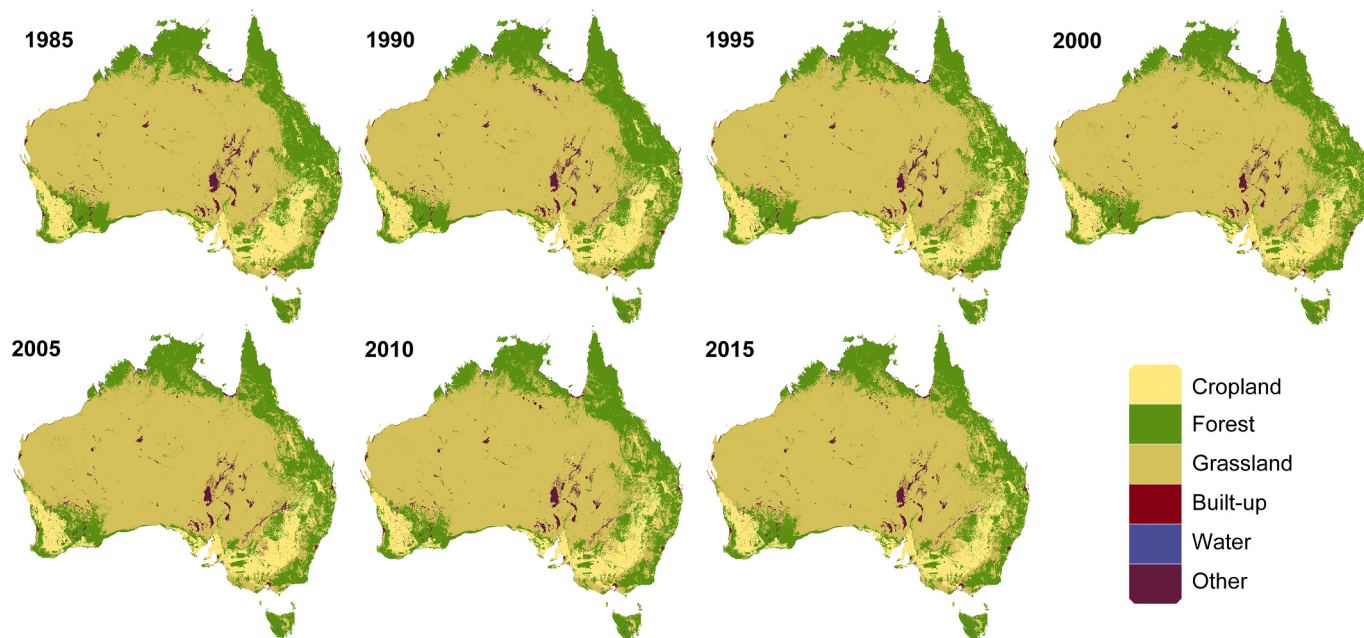


Fig. 3. Australia's land-cover classification maps from 1985 to 2015. (2 columns).

Table 5
Error matrix of validation points ($n = 9140$) for Australia's 2000 land-cover classification.

	Cropland	Forest	Grassland	Built-up	Water	Other	Total	UA (%)	CE (%)
Cropland	2072	31	88	7	15	6	2219	93.4	6.6
Forest	23	2274	65	12	3	0	2377	95.7	4.3
Grassland	81	135	1108	8	5	14	1351	82.0	18.0
Built-up	3	1	7	2110	1	4	2126	99.2	0.8
Water	3	0	0	0	838	2	843	99.4	0.6
Other	2	1	17	4	13	187	224	83.5	16.5
Total	2184	2442	1285	2141	875	213	9140		
PA (%)	94.9	93.1	86.2	98.6	95.8	87.8			
OE (%)	5.1	6.9	13.8	1.4	4.2	12.2			

Where: PA: Producer Accuracy; UA: User Accuracy; CE: Commission Errors; OE: Omission errors.

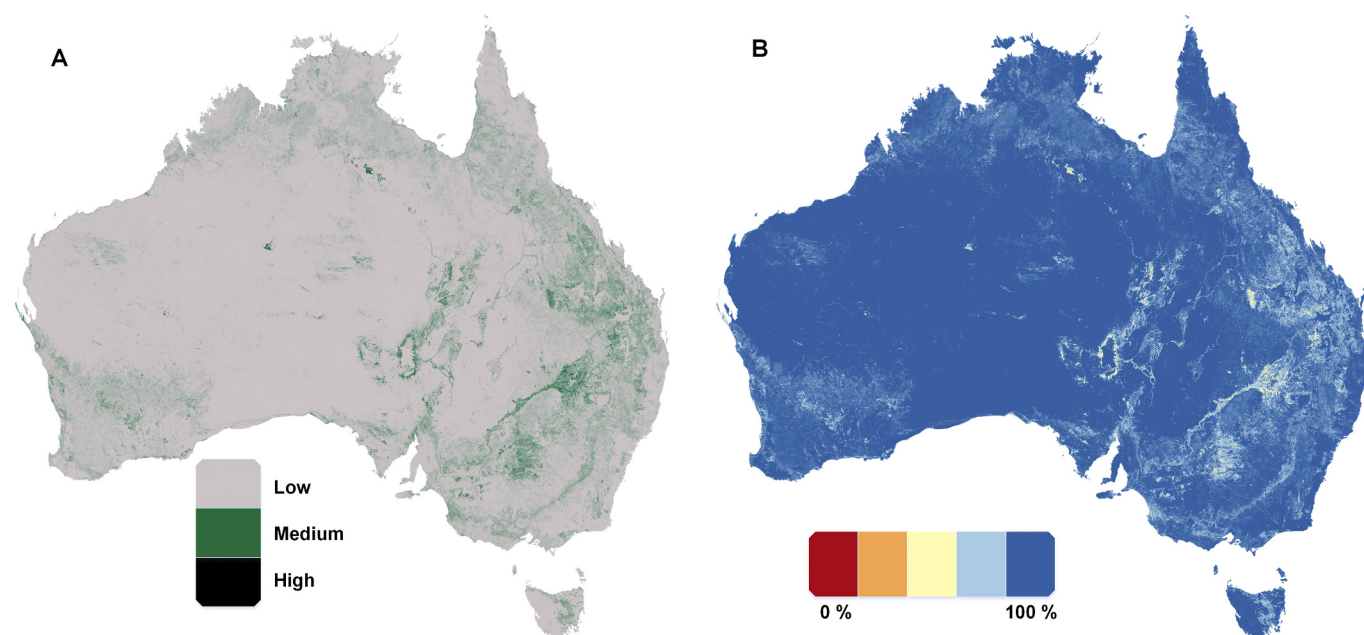


Fig. 4. Per-pixel land-cover classification uncertainty for 2015 calculated using Shannon entropy (A) (Eq. 14) and margin of victory (B). (2 column width).

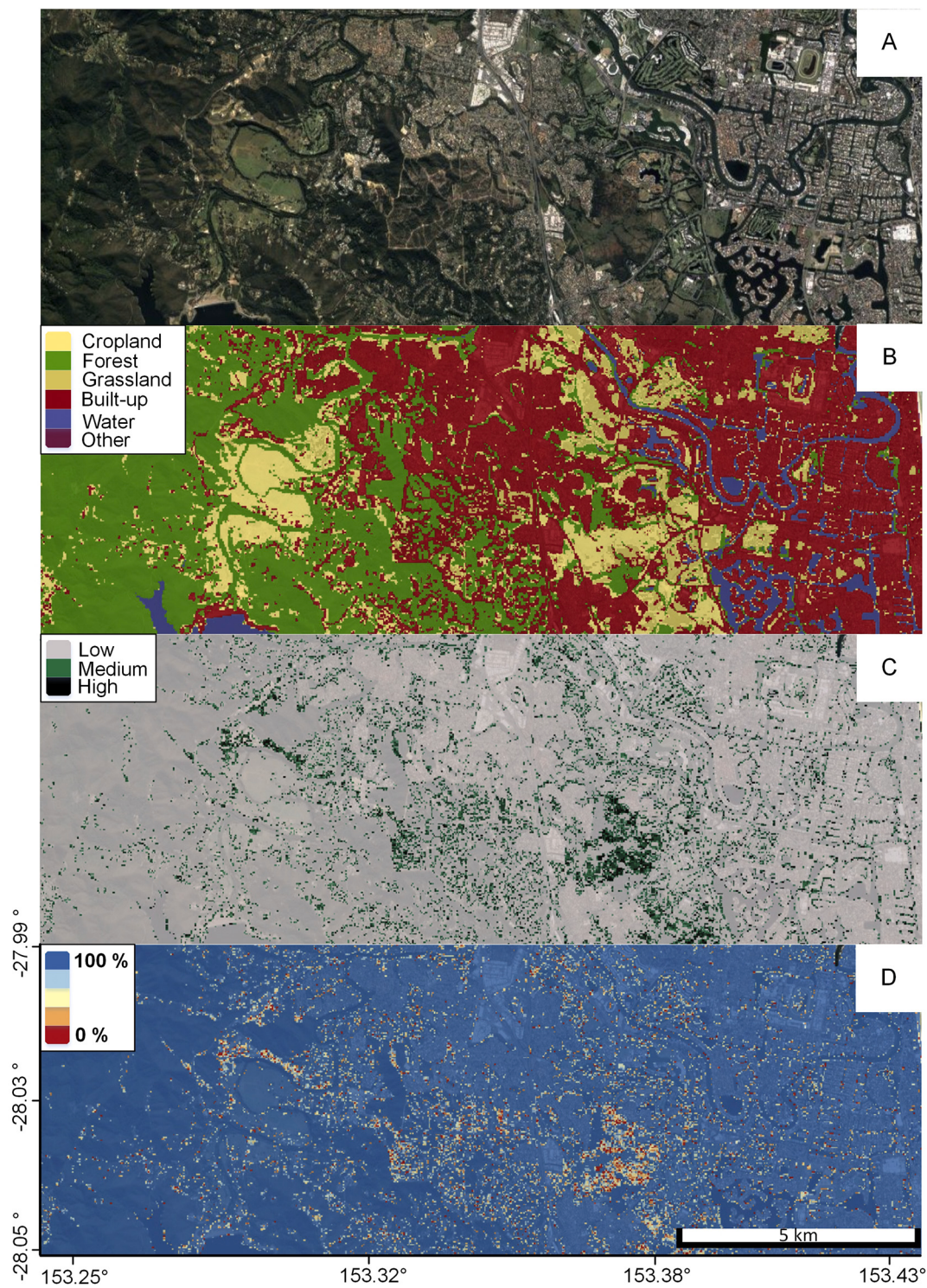


Fig. 5. Detailed overview of the 2015' Gold Coast, Southeast Queensland (A), land-cover classification (B). Per-pixel uncertainty is low in homogenous landscapes, entropy level (C) and margin of victory (D). Background image source: Google Earth 2019 ®. (2 columns). (For interpretation of the references to colour in this figure legend, the reader is referred to the web version of this article.)

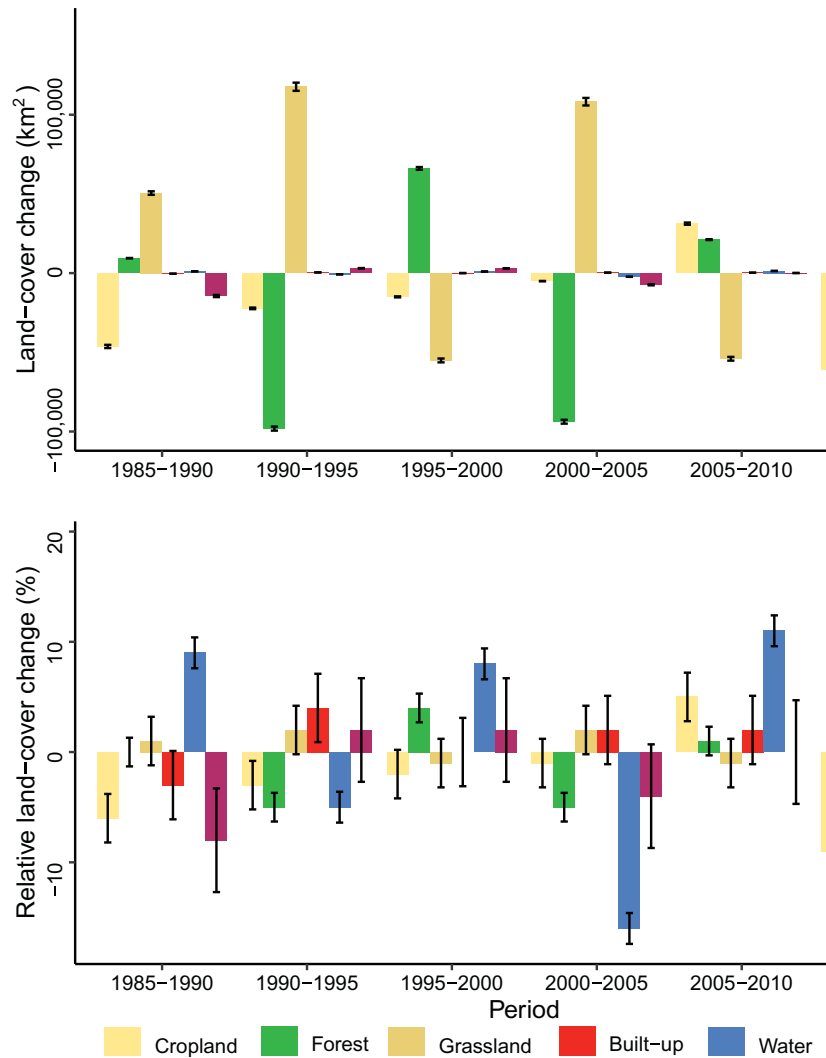
From a temporal perspective, absolute changes in land-cover were found to be higher from 1990 to 2000 and from 2010 to 2015 (Fig. 6A). At land-cover class level, transitions occurred at different rates depending on the land-cover class. For instance, the largest Cropland losses were concentrated at the beginning and at the end of the study period, whereas Cropland expansion was captured during 2005–2010 (Fig. 6B). In general, Grassland experienced gains across the years that were related to losses in other land-cover classes and to its higher

omission and commission errors (Table 6). Built-up area growth had its peak during the last five years of our study, with a relative growth >15% when compared to the preceding time-step. Similarly, at the national level Forest losses occurred mostly between 1990 and 1995, 2000–2005, and 2010–2015. Other areas, experienced a large (~−8%) decline at the beginning of the study period, later incorporated mainly into Grasslands.

The sensitivity for capturing change in land-cover at the national

Table 6Transition matrix for six land-cover classes from 1985 to 2015 (units: km²).

1985	2015	Cropland	Forest	Grassland	Built-up	Water	Other	Area 1985	Δ Area-adj (%) and 95% CI (%)
Cropland	539,258	55,452	148,334	1467	924	7516	752,951	-8.6 (± 2.2)	
Forest	44,924	1,567,712	327,765	1429	753	3604	1,946,186	-7.8 (± 1.3)	
Grassland	44,256	132,288	4,575,506	2152	471	20,851	4,775,523	0.8 (± 2.2)	
Built-up	721	1036	674	9812	37	40	12,320	19.2 (± 3.1)	
Water	884	357	317	55	10,374	941	12,928	5.8 (± 1.4)	
Other	4,866	2662	41,481	98	1206	130,148	180,460	-14.8 (± 4.7)	
Area 2015	634,908	1,759,508	5,094,076	15,013	13,765	163,100			

**Fig. 6.** Land-cover change and 95% confidence intervals in absolute terms (A) and per-land-cover class (B) for 1985–2015. (1.5 columns).

level was 96.4%, whereas the specificity for representing no-change was 68.3% (Table 7). In general, the ability for capturing change was higher than the specificity for representing stable areas across the six reference locations, > 90% and > 56.5% respectively. In the Built-up/Forest dominated area (Fig. 7A) the sensitivity for capturing change in land-cover was 100% and the specificity for representing no-change was 81.1% (the highest across areas). Heterogeneous landscapes with a combination of sparse vegetation, open forests and croplands (Fig. 7B, Fig. 7D and Fig. 7E) presented specificities lower than 70%, i.e., land-cover change was overrepresented by more than 30%.

4. Discussion

We have developed a consistent time-series of seven high spatial resolution (30-m) land-cover and uncertainty maps for the period 1985–2015 for continental Australia. We show that an error-adjusted area of 510,975 km² ($\pm 69,877$ km²) of Australian land changed at a rate of 17,033 km² yr⁻¹ (± 2329 km² yr⁻¹). 1990–1995 and 2010–2015 were the periods of greatest change, experiencing 242,354 km² and 307,647 km² of change, respectively. Among land-cover classes, Built-up areas presented the highest relative increases in area, growing by 2362 km² (± 72.6 km²) at a rate of ~79 km² yr⁻¹ (± 2.4 km² yr⁻¹),

Table 7

Binary confusion matrix for land-cover change accuracy assessment at national level and for the six assessed focal areas for 1985–2015.

	Change	No-change	Total	Sensitivity (%)	Specificity (%)	Prevalence (%)
National						
Change	509	399	908	96.4	68.6	29.3
No-change	19	873	892			
Total	528	1272				
A. Perth: Built-up/Forest				100	81.1	47
Change	141	30	171			
No-change	0	129	129			
Total	141	159				
B. Darwin: Built-up/Forest				90.7	68.5	14
Change	39	81	120			
No-change	4	176	180			
Total	43	257				
C. Alice Springs: Built-up/Grassland				98.8	71.2	28
Change	84	62	146			
No-change	1	153	154			
Total	85	215				
D. Queensland: Forest/Grassland				93.3	63.8	30
Change	84	76	160			
No-change	6	134	140			
Total	90	210				
E. Melbourne: Built-up/Forest/Cropland				96.5	56.5	38
Change	110	81	191			
No-change	4	105	109			
Total	114	186				
F. Hobart: Forest/Built-up/Cropland				92	71.8	18
Change	51	69	120			
No-change	4	176	180			
Total	55	245				

whereas Forests experienced the biggest losses over the period of $152,492 \text{ km}^2 (\pm 24,749 \text{ km}^2)$ at $-5083 \text{ km}^2 \text{ yr}^{-1} (\pm 825 \text{ km}^2 \text{ yr}^{-1})$. The high overall accuracy of our estimates ($>90\%$) and the explicit per-pixel uncertainty at each time-step provides the necessary confidence in the validity of the maps and their role in understanding land change in Australia at high-spatial resolution and over a long time-frame.

4.1. Interpretation of land change in Australia

Land change has occurred heterogeneously across Australia and between land-cover classes. For instance, Croplands continuously declined in area until 2005 when Grassland transitioned to Cropland and Forest, increasing Cropland extent mainly in Queensland and Victoria. Increases in population and population density, access to markets, and climate conditions are likely to have influenced these cropland dynamics (Lesslie and Mewett, 2018; Marcos-Martinez et al., 2017). Similarly, peak Forest losses were recorded every ten years from 1990 to 1995 onwards principally changing to Grasslands and Croplands. Wildfires, and deforestation driven by agriculture, forestry, and urbanization have acted as the main drivers of tree cover loss in Australia over the past 15 years (Curtis et al., 2018). The main hotspots of land clearance have been located in Queensland, Northern Territory, and Western Australia (Supplementary Materials, Table S4), with the expansion or contraction of Forests being directly related to laws and policies that encourage/discourage land clearing activities (Simmons et al., 2018a, 2018b, 2018c). At around $-5083 \text{ km}^2 \text{ yr}^{-1}$, our trends of deforestation at the national level are higher than the $\sim 2700 \text{ km}^2 \text{ yr}^{-1}$ estimated by Evans (2016). The presence of temporal inconsistencies, especially in our 1985 and 1990 land-cover maps where omission and commission errors were larger for Grasslands and Forests, respectively (see Table S3), may have contributed to this difference.

Our definition of Grassland included pastures (managed and unmanaged), chenopods, tussock grasses, and hummock grasses covering around 66% of the Australian land mass and making this class the dominant land-cover class in the country. Changes in Grasslands appeared to be a response to changes in other land-cover classes. At the national level, Grassland increased in extent because of losses in Forest

and Cropland (Table 6 and Fig. 6). Other areas were also converted to Grassland, but this may have been related to classification errors in addition to actual land change. In localised areas the opposite trend was found with increases in Built-up areas encroaching into Grassland (Fig. 7A, C & E).

Built-up areas experienced the highest relative increases across the country at around 19% over the study period. Increases in population coupled with low population densities, growth in GDP and incentives for infrastructure construction have all influenced the magnitude and direction of urban growth (McDonald et al., 2013; Seto et al., 2011). At the state level, Built-up area increases ranged from $>11\%$ in Tasmania to 54% in the Australian Capital Territory. Urban growth has mostly encroached into Grassland, Cropland, and Forest. Major Grassland losses due to Built-up area expansion ($-2152 \text{ km}^2, \pm 66.7 \text{ km}^2$) were observed in Victoria ($-870 \text{ km}^2, \pm 27 \text{ km}^2$), New South Wales ($-393 \text{ km}^2, \pm 12.2 \text{ km}^2$), and Western Australia ($-368 \text{ km}^2, \pm 11.4 \text{ km}^2$), respectively. Built-up area growth led to Forest losses in Queensland ($-543 \text{ km}^2, \pm 16.8 \text{ km}^2$) and New South Wales ($-331 \text{ km}^2, \pm 10.3 \text{ km}^2$). The encroachment of Built-up land into Cropland was also prominent in these two states (Supplementary Materials, Table S4). At the local level, urban growth also varied. Perth's urban expansion (Fig. 7A) has been fairly evenly distributed in all inland directions encroaching into Forest and Cropland areas, whereas Melbourne (Fig. 7E) increased its urban extent mainly towards the northwest into Grassland. To the best of our knowledge, urban growth has not been quantified at this resolution for Australia before and this assessment provides the most comprehensive depiction of complex patterns of urban expansion and the land changes associated with it.

Water presented 5.8% ($\pm 1.4\%$) increase in area from 1985 to 2015. This apparent increase is most likely to result from temporal dynamics in lake area resulting for seasonal wetting and drying (e.g., salt lakes). Other areas also displayed increases, but it was not possible to discriminate between classification error and actual changes as these areas were commonly confused with other land-cover classes (Table 6).

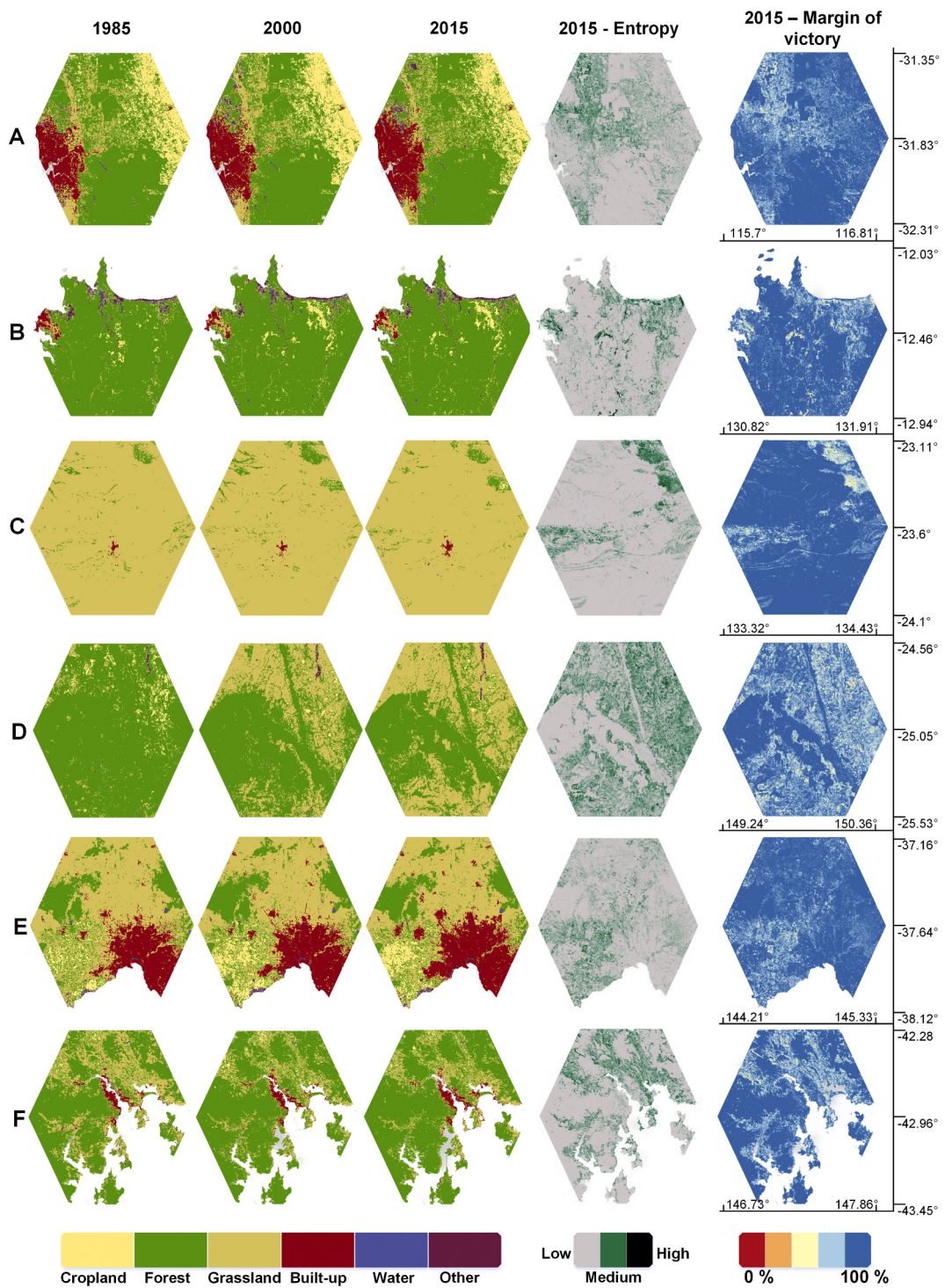


Fig. 7. Results of land-cover transition assessment at the six sites. A) Perth city and its buffer zone; B) Darwin city and its surrounding area; C) Alice Springs city and its hinterland; D) Forest-Grassland transition area in Queensland; E) Melbourne and its hinterland; and, F) Hobart city and its surrounding landscape. (2 column width).

4.2. Land-cover classification a comparison

Our estimates of land-cover extent for every class differed with the extents reported by the DLCD v2.1 map (Table 8). Except for Forest, Grassland, and Built-up areas, relative differences in the other three classes were higher than 50%, with Cropland area being almost twice as large as the area reported by the DLCD. Thematic resolution, land-cover class typology, spatial resolution, sensor sensitivity, land-cover

classification, and the absence of temporal postprocessing methods in our land-cover maps all contribute to these differences (Alexander et al., 2016b; Prestele et al., 2016; Scarth et al., 2015). The influence of each of these factors is discussed in Section 4.4.

New studies at high-spatial resolution are offering new insights of land-cover extent. For example, recent figures produced by Scarth et al. (2019) at 30-m resolution estimated Forest extent (including Forests and woodlands with height over 5 m and a crown cover over 20%) at

Table 8

Land-cover area comparison for 2010 between the Dynamic Land Cover Dataset (DLCD v2.1) and this study.

	DLCD (km ²)	This study (km ²)	Difference (km ²)	Relative difference (%)
Cropland	354,939	695,609	340,670	96.0
Forest	1,827,314	1,850,897	23,583	1.3
Grasslands	5,530,179	4,942,774	-587,405	-10.6
Built-up	10,191	12,997	2806	27.5
Water	33,269	13,350	-19,919	-59.9
Other	109,448	164,734	-55,285	50.5

~1,685,000 km² for 2010, similar to our estimates for the same year of 1,850,897 km². Teluguntla et al. (2018) reported a cropland extent of ~351,000 km² using 30-m satellite imagery for 2015, the figure increased to around 657,000 km² when they incorporated pasture in the analysis. In comparison, we estimated an extent of 634,908 km² for cropland in 2015 (Table 6). Differences in Cropland extent may have been influenced by the 5-year time window employed in this study for constructing the raw mosaics which would result in crop-rotation areas and mixed-farming areas being captured as croplands.

4.3. Potential application of data and methods, and caveats

Our results provide a comprehensive set of historical wall-to-wall land-cover and uncertainty data layers and land change information for Australia. Until now, national land-cover information for Australia was available only at coarse-spatial resolution (e.g., Bontemps et al., 2013; Friedl et al., 2010; Lymburner et al., 2011), or for limited time slices (e.g., Chen et al., 2015) and lacked confidence information at pixel level. While there are a growing number of studies employing high-spatial resolution information at a national and continental level, for Australia these are mainly monothematic e.g., cropland vs non-cropland (Teluguntla et al., 2018) or vegetation vs non-vegetation (Scarth et al., 2019). Studies using historical multiclass information at finer resolution have been limited to local geographical areas (e.g., South Australian Department for Environment and Water, 2018), hindering the understanding of teleconnected processes and drivers across larger extents and increasing the uncertainty of future land-cover projections. The high resolution and accuracy of our maps together with the per-pixel confidence layers make them suitable as inputs of high spatiotemporal resolution land change simulation models for unravelling the main drivers of these changes and for projecting land change into the future (e.g. Liu et al., 2017; Roodposhti et al., 2019). In addition, due to the time-span and grain of analysis, this comprehensive resource can be useful for planners and policymakers undertaking land-management planning, and for researchers requiring prompt and accurate information on land-cover and land change as inputs into studies spanning a wide range of purposes including greenhouse gas emissions, food security, sustainability, and biodiversity assessments. An additional application of these maps is in updating historical fractional land-cover products, the spatial information of the maps can be easily aggregated at different spatial levels for representing the proportion of every land-cover class inside a pixel.

The methodological framework employed, cloud-based and local, for our mapping provides a robust and efficient approach for producing land-cover information over large areas can be readily adapted, refined, and applied elsewhere as it. Until now, multiclass time-series information at this spatial extent and resolution has been limited to a few regions around the globe and lacked uncertainty information at a spatial level (Hu and Hu, 2019; MapBiomas, 2019; Midekisa et al., 2017). Furthermore, while studies have used outlier detection methods for increasing the accuracy of the pseudo ground-truth data (Hu and Hu, 2019; Vidal-Macua et al., 2017), most studies have not performed any quality assurance check of their reference data (Pelletier et al., 2017). Here, we were able to analyze and classify ~281,962 satellite images (~90 terabytes) in GEE, almost 30 times more than the amount of images needed

for representing global land-cover at one time-step (Giri et al., 2013), in a matter of months. Additionally, we have implemented an interactive semi-automated method that reduces the amount of resources involved in the construction of historically-consistent pseudo ground-truth data, and, incorporated two per-pixel accuracy metrics for uncertainty assessment. This same logic could be applicable to nations, continents, and regions with similar or even larger area in a manageable time period.

While we have made every effort to make the landcover mapping process transparent, reproducible, and the error and uncertainty explicit, significant limitations persist. First, although GEE offers a proprietary cloud-computing service, free for research purposes, with unparallel capabilities for handling and analyzing petabytes of geo-spatial information, as part of the terms of service, GEE may add, modify, or deprecate any of its analytical algorithms or functions which might alter the performance of the analysis (we recommend readers keep abreast of the latest updates in GEE by referring to the API changelog, <https://developers.google.com/earth-engine/changelog>) or even preclude future replication. Similarly, future reproducibility of the current research will also depend on the existence of remote GEE servers. Studies at smaller scales should consider the use of historical stable archives (e.g., USGS EROS) and reproducible workflows.

4.4. Accuracy, uncertainty, and its sources

Besides substantially enhancing the spatial and temporal resolution of the available land-cover information for Australia, our mapping product offers per-pixel confidence information unavailable at national level until now. Our classification performed better for Built-up and Water classes (producer and user accuracy >95%) whereas Grassland and Other areas presented the lowest accuracies (producer and user accuracy >82%). Furthermore, the land-cover extent of every class was unbiased. The omission and commission errors presented similar magnitudes for every class, except for Water where omission errors were slightly higher (i.e., maps identified less area of water bodies than their actual extent), suggesting no systematic under or overestimation. Over time, land-cover maps presented higher omission and commission errors for Grasslands and Forests. Land-cover change accuracy expressed as sensitivity and specificity, differed between the six sites assessed (Table 7). Although land change is overrepresented in the six areas, areas with lower specificity (<70%) occurred in heterogeneous landscapes dominated by Forest, Grassland, and Cropland mosaics (Fig. 7B, D and E). The highest land change overrepresentation was found for Forest, i.e., an overestimation of deforestation illustrated by a specificity 62.2% (Table S5). This highlights the importance of implementing a post-classification process for reducing the omission and commission errors, ensuring the temporal consistency and improving the land-change accuracy of the classified maps. We note though that due to the very many ways of doing this we have preferred to present the maps in as raw a form as possible and leave postprocessing to users to suit their own requirements.

Sources of lower accuracies (in the case of Grasslands and Other areas), commission and omission errors, and land-cover change errors are related to the: 1) definition of land-cover classes; 2) reliability of the satellite imagery and sensor limitations; 3) ancillary variables for land-cover classification; and, 4) mislabeled training and validation data. We defined our land-cover classes based on the purpose of our mapping, the land-cover classification used as a reference, accepted definitions, technical capabilities of Landsat sensors, and the available information for discriminating similar classes (e.g., Grassland and Cropland). In this context, there is a trade-off between the reliability of the classifier for capturing differentiable classes (e.g., Built-up areas) and those that present similar spectral characteristics (e.g., Grasslands and Croplands). Furthermore, Grasslands and Other areas contain a vast array of spectrally similar sub-classes. For instance, from visual assessment we found common confusion between areas with sparse vegetation and Grasslands

(in some areas those are classified as Forest and in other as Grasslands). Similarly, Other areas (that included salt lakes, bare lands, mines, sand dunes, and wetlands) were often classified as Water, Built-up, or Grassland. While the addition of bioclimatic information (e.g., precipitation and mean temperature) and spectral indices (e.g., EVI, NDWI) at a seasonal level helped to improve the consistency of the classifications, further post-processing is required. Despite the temporal and spectral resolution of Landsat sensors, we managed to have cloud-free and shadow-free composites for every time-step. Because of the size of our study area, computation time and memory limitations in GEE, we restricted the number of ancillary variables ($n = 49$), descriptive statistics (we used only the median), seasons ($n = 7$), training ($n = 19,552$) and validation points ($n = 9178$), and, the number of k-folds ($k = 10$) used in the classification process. Although we tested the performance of the classification with different sets of variables on a local computer, we may have omitted/included relevant/redundant variables that could have influenced the final classifications. While increasing the training sample size and the number of folds used in the classification may further increase the accuracy of our results, the effect is likely to be marginal.

Our interactive semi-automated method for constructing an historical set of invariant pseudo-ground truth data performed adequately as we clustered pixels with similar spectral characteristics and retained those that did not change during the period of study. The process had to be complemented with a visual validation for reducing the maximum number of mislabeled pixels, and for ensuring a homogeneous distribution across the country and a robust training and validation dataset. Subjectivity at the moment of deciding the reference class of a pixel could have introduced noise in the training and validation datasets, however, the impact of noise on the final classification should be low (Zhu et al., 2016). A lack of 'true' complex pixels (Nguyen and Henebry, 2019) in the training dataset might also have influenced the confusion between classes in heterogeneous landscapes. The use of machine learning methods may help to automate the process of constructing pseudo-ground truth datasets and reduce labeling costs (Heremans et al., 2011).

Each land-cover map has an associated entropy and margin of victory map (Fig. 4). We used the two measures as a proxy of per-pixel-classification confidence (Brown et al., 2009; Khatami et al., 2017; Shadman Roodposhti et al., 2019b). These maps provide useful information about the stability of the classifications as well as the areas with higher uncertainty (i.e., high entropy and low margin of victory, e.g., in Queensland Fig. 7D). We strongly suggest to use this information for making use of these maps for posterior analyses. In addition, per-pixel confidence maps provide information about the areas where more ground-truth data might be needed. Areas with high uncertainty were similar across the years and were usually concentrated in heterogeneous landscapes or in small patches.

5. Conclusion

We have presented a historical set of seven wall-to-wall land-cover maps for Australia at 30-m resolution at 5-year time steps from 1985 to 2015. The maps are the first-of-their-kind for Australia, and one of only a few available at continental scale. They were created by using more than 281,962 Landsat scenes and have an overall accuracy of ~93%. Per-class producer and user accuracies were above 90% for most land-cover classes illustrating the confidence of our estimates. The results show that ~6.7% ($\pm 0.9\%$) of the Australian land mass has experienced land change at a rate of $\sim 17,033 \text{ km}^2 \text{ yr}^{-1}$ ($\pm 2329 \text{ km}^2 \text{ yr}^{-1}$). While the main losses occurred in Croplands and Forests, the highest relative increases were experienced by Built-up areas coming mainly at the expense of Grassland losses. Accuracy assessment suggested that the sensitivity for capturing change was 96.4%, whereas the specificity for representing stable areas was 68.3%, i.e., change was erroneously simulated in areas dominated by a mosaic of Forest (especially open forests and tall

woodlands), Grassland (tall shrublands), and Cropland. These results can be combined with the uncertainty maps for the design and implementation of postprocessing rules depending on the final users' needs. Similarly, these outputs can be used for identifying areas that require more ground-truth data. By exploiting the capabilities of GEE for analyzing big geospatial data, we have demonstrated that time-series mapping of land-cover over large areas at high-spatial resolution is now possible. This land change assessment framework is suitable for understanding land dynamics at large extents. Our freely-available maps provide a consistent data product for the assessment of land change at local to national scales and as inputs for a plethora of other modelling exercises and assessments.

Authors responsibilities

The concept of this research was initially developed by MCL, MH, and BB. MCL designed and performed the classification and analyses and wrote the initial draft of the paper. MCL, MH and BB contributed for the interpretation of the findings and edited the paper.

Funding

This research was supported by the funding from the Deakin University Postgraduate Research Scholarship (0000019085) and the Australian Research Council Discovery (DP170104795), funded by the Australian Government.

Declaration of Competing Interest

The authors declare that they have no known competing financial interests or personal relationships that could have appeared to influence the work reported in this paper.

Appendix A. Supplementary data

Supplementary data to this article can be found online at <https://doi.org/10.1016/j.rse.2020.112148>.

References

- ABARES, 2016. The Australian Land Use and Management Classification Version 8. Australian Bureau of Agricultural and Resource Economics and Sciences, Canberra, 3.0.
- Alexander, P., Brown, C., Arneth, A., Finnigan, J., Rounsevell, M.D.A., 2016a. Human appropriation of land for food: the role of diet. *Glob. Environ. Chang.* 41, 88–98.
- Alexander, P., Prestele, R., Verburg, P.H., Arneth, A., Baranzelli, C., Batista, E.S.F., Brown, C., Butler, A., Calvin, K., Dendoncker, N., Doelman, J.C., Dunford, R., Engstrom, K., Eitelberg, D., Fujimori, S., Harrison, P.A., Hasegawa, T., Havlik, P., Holzhauser, S., Humpenoder, F., Jacobs-Crisioni, C., Jain, A.K., Krisztin, T., Kyle, P., Lavalle, C., Lenton, T., Liu, J., Meiyappan, P., Popp, A., Powell, T., Sands, R.D., Schaldach, R., Stehfest, E., Steinbuks, J., Tabaei, A., van Meijl, H., Wise, M.A., Rounsevell, M.D., 2016b. Assessing uncertainties in land cover projections. *Glob. Chang. Biol.* 23, 767–781.
- Ali, I., Cawkwell, F., Dwyer, E., Barrett, B., Green, S., 2016. Satellite remote sensing of grasslands: from observation to management. *J. Plant Ecol.* 9, 649–671.
- Arino, O., Gross, D., Ranera, F., Leroy, M., Bicheron, P., Brockman, C., Defourny, P., Vancutsem, C., Achard, F., Durieux, L., 2007. GlobCover: ESA service for global land cover from MERIS. In: 2007 IEEE International Geoscience and Remote Sensing Symposium. IEEE, pp. 2412–2415.
- Australian Bureau of Statistics, 2016. Urban Centres and Localities (UCL). Australian Bureau of Statistics. <https://www.abs.gov.au/websitedbs/D3310114.nsf/home/Digital+Boundaries>.
- Bengio, Y., Grandvalet, Y., 2004. No unbiased estimator of the variance of k-fold cross-validation. *J. Mach. Learn. Res.* 5, 1089–1105.
- Bonan, G.B., 2008. Forests and climate change: forcings, feedbacks, and the climate benefits of forests. *Science* 320, 1444–1449.
- Bontemps, S., Defourny, P., Radoux, J., Van Bogaert, E., Lamarche, C., Achard, F., Mayaux, P., Boettcher, M., Brockmann, C., Kirches, G., 2013. Consistent global land cover maps for climate modelling communities: current achievements of the ESA's land cover CCI. In: Proceedings of the ESA Living Planet Symposium, Edinburgh, pp. 9–13.
- Bossard, M., Feranec, J., Otahel, J., 2000. CORINE Land Cover Technical Guide: Addendum, p. 2000.
- Breiman, L., 2001. Random forests. *Mach. Learn.* 45, 5–32.

- Brown, K.M., Foody, G.M., Atkinson, P.M., 2009. Estimating per-pixel thematic uncertainty in remote sensing classifications. *Int. J. Remote Sens.* 30, 209–229.
- Brown, D.G., Verburg, P.H., Pontius, R.G., Lange, M.D., 2013. Opportunities to improve impact, integration, and evaluation of land change models. *Curr. Opin. Environ. Sustain.* 5, 452–457.
- Bryan, B.A., Nolan, M., McKellar, L., Connor, J.D., Newth, D., Harwood, T., King, D., Navarro, J., Cai, Y., Gao, L., Grundy, M., Graham, P., Ernst, A., Dunstall, S., Stock, F., Brinsmead, T., Harman, I., Grigg, N.J., Battaglia, M., Keating, B., Wonhas, A., Hatfield-Dodds, S., 2016. Land-use and sustainability under intersecting global change and domestic policy scenarios: trajectories for Australia to 2050. *Glob. Environ. Chang.* 38, 130–152.
- Carlotto, M.J., 2009. Effect of errors in ground truth on classification accuracy. *Int. J. Remote Sens.* 30, 4831–4849.
- Carlson, T.N., Ripley, D.A., 1997. On the relation between NDVI, fractional vegetation cover, and leaf area index. *Remote Sens. Environ.* 62, 241–252.
- Chen, J., Chen, J., Liao, A., Cao, X., Chen, L., Chen, X., He, C., Han, G., Peng, S., Lu, M., Zhang, W., Tong, X., Mills, J., 2015. Global land cover mapping at 30m resolution: a POK-based operational approach. *ISPRS J. Photogramm. Remote Sens.* 103, 7–27.
- Congalton, R., Gu, J., Yadav, K., Thenkabail, P., Ozdogan, M., 2014. Global land cover mapping: a review and uncertainty analysis. *Remote Sens.* 6, 12070–12093.
- Curtis, P.G., Slay, C.M., Harris, N.L., Tyukavina, A., Hansen, M.C., 2018. Classifying drivers of global forest loss. *Science* 361, 1108–1111.
- Denisko, D., Hoffman, M.M., 2018. Classification and interaction in random forests. *Proc. Natl. Acad. Sci.* 115, 1690–1692.
- Diek, S., Fornallaz, F., Schaepe, M., de Jong, R., 2017. Barest pixel composite for agricultural areas using landsat time series. *Remote Sens.* 9, 1245.
- Evans, M.C., 2016. Deforestation in Australia: drivers, trends and policy responses. *Pac. Conserv. Biol.* 22, 130–150.
- Farr, T.G., Rosen, P.A., Caro, E., Crippen, R., Duren, R., Hensley, S., Kobrick, M., Paller, M., Rodriguez, E., Roth, L., 2007. The shuttle radar topography mission. *Rev. Geophys.* 45.
- Foley, J.A., DeFries, R., Asner, G.P., Barford, C., Bonan, G., Carpenter, S.R., Chapin, F.S., Coe, M.T., Daily, G.C., Gibbs, H.K., Helkowski, J.H., Holloway, T., Howard, E.A., Kucharik, C.J., Monfreda, C., Patz, J.A., Prentice, I.C., Ramankutty, N., Snyder, P.K., 2005. Global consequences of land use. *Science* 309, 570–574.
- Foody, G.M., 2002. Status of land cover classification accuracy assessment. *Remote Sens. Environ.* 80, 185–201.
- Foody, G.M., 2010. Assessing the accuracy of land cover change with imperfect ground reference data. *Remote Sens. Environ.* 114, 2271–2285.
- Foody, G.M., Mathur, A., 2006. The use of small training sets containing mixed pixels for accurate hard image classification: training on mixed spectral responses for classification by a SVM. *Remote Sens. Environ.* 103, 179–189.
- Friedl, M.A., Sulla-Menashe, D., Tan, B., Schneider, A., Ramankutty, N., Sibley, A., Huang, X., 2010. MODIS collection 5 global land cover: algorithm refinements and characterization of new datasets. *Remote Sens. Environ.* 114, 168–182.
- Giri, C., Pengra, B., Long, J., Loveland, T.R., 2013. Next generation of global land cover characterization, mapping, and monitoring. *Int. J. Appl. Earth Obs. Geoinf.* 25, 30–37.
- Gong, P., Liu, H., Zhang, M., Li, C., Wang, J., Huang, H., Clinton, N., Ji, L., Li, W., Bai, Y., Chen, B., Xu, B., Zhu, Z., Yuan, C., Ping Suen, H., Guo, J., Xu, N., Li, W., Zhao, Y., Yang, J., Yu, C., Wang, X., Fu, H., Yu, L., Dronova, I., Hui, F., Cheng, X., Shi, X., Xiao, F., Liu, Q., Song, L., 2019. Stable classification with limited sample: transferring a 30-m resolution sample set collected in 2015 to mapping 10-m resolution global land cover in 2017. *Sci. Bull.* 64, 370–373.
- Gorelick, N., Hancher, M., Dixon, M., Ilyushchenko, S., Thau, D., Moore, R., 2017. Google earth engine: planetary-scale geospatial analysis for everyone. *Remote Sens. Environ.* 202, 18–27.
- Grundy, M.J., Bryan, B.A., Nolan, M., Battaglia, M., Hatfield-Dodds, S., Connor, J.D., Keating, B.A., 2016. Scenarios for Australian agricultural production and land use to 2050. *Agric. Syst.* 142, 70–83.
- Guershman, J.P., Hill, M.J., Renzullo, L.J., Barrett, D.J., Marks, A.S., Botha, E.J., 2009. Estimating fractional cover of photosynthetic vegetation, non-photosynthetic vegetation and bare soil in the Australian tropical savanna region upscaling the EO-1 Hyperion and MODIS sensors. *Remote Sens. Environ.* 113, 928–945.
- Güneralp, B., Seto, K., 2013. Futures of global urban expansion: uncertainties and implications for biodiversity conservation. *Environ. Res. Lett.* 8, 014025.
- Güneralp, B., Seto, K.C., Ramachandran, M., 2013. Evidence of urban land teleconnections and impacts on hinterlands. *Curr. Opin. Environ. Sustain.* 5, 445–451.
- Hansen, M.C., Defries, R.S., Townshend, J.R.G., Sohlberg, R., 2000. Global land cover classification at 1 km spatial resolution using a classification tree approach. *Int. J. Remote Sens.* 21, 1331–1364.
- Hansen, M.C., Potapov, P.V., Moore, R., Hancher, M., Turubanova, S.A., Tyukavina, A., Thau, D., Stehman, S.V., Goetz, S.J., Loveland, T.R., Kommareddy, A., Egorov, A., Chini, L., Justice, C.O., Townshend, J.R., 2013. High-resolution global maps of 21st-century forest cover change. *Science* 342, 850–853.
- Hasegawa, T., Fujimori, S., Ito, A., Takahashi, K., Masui, T., 2017. Global land-use allocation model linked to an integrated assessment model. *Sci. Total Environ.* 580, 787–796.
- Heck, V., Hoff, H., Wirsénus, S., Meyer, C., Kreft, H., 2018. Land use options for staying within the planetary boundaries – Synergies and trade-offs between global and local sustainability goals. *Glob. Environ. Chang.* 49, 73–84.
- Heremans, S., Bosmans, B., Eerens, H., Van Orshoven, J., 2011. Efficient collection of training data for sub-pixel land cover classification using neural networks. *Int. J. Appl. Earth Obs. Geoinf.* 13, 657–667.
- Hijmans, R.J., van Etten, J., 2016. Raster: Geographic Data Analysis and Modeling. R package version 2.8.
- Hijmans, R., Cameron, S., Parra, J., Jones, P., Jarvis, A., 2004. The WorldClim Interpolated Global Terrestrial Climate Surfaces. Version 1.3.
- Hoskins, A.J., Bush, A., Gilmore, J., Harwood, T., Hudson, L.N., Ware, C., Williams, K.J., Ferrier, S., 2016. Downscaling land-use data to provide global 30° estimates of five land-use classes. *Ecol. Evol.* 6, 3040–3055.
- Hu, Y., Hu, Y., 2019. Land cover changes and their driving mechanisms in Central Asia from 2001 to 2017 supported by Google earth engine. *Remote Sens.* 11, 554.
- Huang, Q., Yang, X., Gao, B., Yang, Y., Zhao, Y., 2014. Application of DMSP/OLS nighttime light images: a meta-analysis and a systematic literature review. *Remote Sens.* 6, 6844–6866.
- Huang, X., Weng, C., Lu, Q., Feng, T., Zhang, L., 2015. Automatic Labelling and selection of training samples for high-resolution remote sensing image classification over urban areas. *Remote Sens.* 7, 15819.
- Huete, A.R., 1988. A soil-adjusted vegetation index (SAVI). *Remote Sens. Environ.* 25, 295–309.
- Huete, A., Liu, H., Batchily, K., Van Leeuwen, W., 1997. A comparison of vegetation indices over a global set of TM images for EOS-MODIS. *Remote Sens. Environ.* 59, 440–451.
- Hurt, G.C., Chini, L.P., Frolking, S., Betts, R.A., Feddema, J., Fischer, G., Fisk, J.P., Hibbard, K., Houghton, R.A., Janetos, A., Jones, C.D., Kindermann, G., Kinoshita, T., Klein Goldewijk, K., Riahi, K., Shevliakova, E., Smith, S., Stehfest, E., Thomson, A., Thornton, P., van Vuuren, D.P., Wang, Y.P., 2011. Harmonization of land-use scenarios for the period 1500–2100: 600 years of global gridded annual land-use transitions, wood harvest, and resulting secondary lands. *Clim. Chang.* 109, 117.
- IPCC, 2014. Climate Change 2014. Contribution of Working Groups I, II and III to the Fifth Assessment Report of the Intergovernmental Panel on Climate Change. IPCC, Geneva, Switzerland.
- Khatami, R., Mountrakis, G., Stehman, S.V., 2017. Mapping per-pixel predicted accuracy of classified remote sensing images. *Remote Sens. Environ.* 191, 156–167.
- Klotz, M., Kemper, T., Geiß, C., Esch, T., Taubenböck, H., 2016. How good is the map? A multi-scale cross-comparison framework for global settlement layers: evidence from Central Europe. *Remote Sens. Environ.* 178, 191–212.
- Koskinen, J., Leinonen, U., Vollrath, A., Ortmann, A., Lindquist, E., d'Annunzio, R., Pekkarinen, A., Kayhkö, N., 2019. Participatory mapping of forest plantations with open Foris and Google earth engine. *ISPRS J. Photogramm. Remote Sens.* 148, 63–74.
- Kuhn, M., 2012. The caret package. In: R Foundation for Statistical Computing. Austria. URL, Vienna. <https://cran.r-project.org/package=caret>.
- Lesslie, R., 2011. Landscapes in Transition: Tracking Land Use Change in Australia. ABARES.
- Lesslie, R., Mewett, J., 2018. Reprint Land Use and Management-The Australian Context, Land Use in Australia. ANU Press, pp. 31–58.
- Liau, A., Wiener, M., 2002. Classification and regression by randomForest. *R News* 2, 18–22.
- Liu, X., Liang, X., Li, X., Xu, X., Ou, J., Chen, Y., Li, S., Wang, S., Pei, F., 2017. A future land use simulation model (FLUS) for simulating multiple land use scenarios by coupling human and natural effects. *Landscape Urban Plan.* 168, 94–116.
- Loveland, T.R., Reed, B.C., Brown, J.F., Ohlen, D.O., Zhu, Z., Yang, L., Merchant, J.W., 2000. Development of a global land cover characteristics database and IGBP DISCover from 1 km AVHRR data. *Int. J. Remote Sens.* 21, 1303–1330.
- Lymburner, L., Tan, P., Mueller, N., Thackway, R., Randall, L., Islam, A., McIntyre, A., Lewis, A., Thankappan, M., Senarath, U., 2011. In: Australia, G. (Ed.), The National Dynamic Land Cover Dataset. ACT, pp. 3297–3300.
- MacLachlan, A., Roberts, G., Biggs, E., Boruff, B., 2017. Subpixel land-cover classification for improved urban area estimates using Landsat. *Int. J. Remote Sens.* 38, 5763–5792.
- MapBiomas, 2019. MapBiomass Project - Is a Multi-institutional Initiative to Generate Annual Land Cover and Use Maps using Automatic Classification Processes Applied to Satellite Images. <http://mapbiomas.org>.
- Marcos-Martinez, R., Bryan, B.A., Connor, J.D., King, D., 2017. Agricultural land-use dynamics: assessing the relative importance of socioeconomic and biophysical drivers for more targeted policy. *Land Use Policy* 63, 53–66.
- Marques, A., Martins, I.S., Kastner, T., Plutzar, C., Theurl, M.C., Eisenmenger, N., Huijbregts, M.A., Wood, R., Stadler, K., Bruckner, M., 2019. Increasing impacts of land use on biodiversity and carbon sequestration driven by population and economic growth. *Nat. Ecol. Evol.* 1.
- Marssett, R.C., Qi, J., Heilman, P., Biedenbender, S.H., Watson, M.C., Amer, S., Weltz, M., Goodrich, D., Marssett, R., 2006. Remote sensing for grassland management in the arid southwest. *Rangel. Ecol. Manag.* 59, 530–540.
- McDonald, R.I., Marcotullio, P.J., Güneralp, B., 2013. Urbanization and Global Trends in Biodiversity and Ecosystem Services, Urbanization, Biodiversity and Ecosystem Services: Challenges and Opportunities. Springer, pp. 31–52.
- McFeeters, S.K., 1996. The use of the normalized difference water index (NDWI) in the delineation of open water features. *Int. J. Remote Sens.* 17, 1425–1432.
- McIver, D.K., Friedl, M.A., 2001. Estimating pixel-scale land cover classification confidence using nonparametric machine learning methods. *IEEE Trans. Geosci. Remote Sens.* 39, 1959–1968.
- Mellor, A., Boukir, S., Haywood, A., Jones, S., 2015. Exploring issues of training data imbalance and mislabelling on random forest performance for large area land cover classification using the ensemble margin. *ISPRS J. Photogramm. Remote Sens.* 105, 155–168.
- Midekisa, A., Holl, F., Savory, D.J., Andrade-Pacheco, R., Gething, P.W., Bennett, A., Sturrock, H.J.W., 2017. Mapping land cover change over continental Africa using Landsat and Google earth engine cloud computing. *PLoS One* 12, e0184926.

- Murray, N.J., Keith, D.A., Simpson, D., Wilshire, J.H., Lucas, R.M., 2018. REMAP: an online remote sensing application for land cover classification and monitoring. *Methods Ecol. Evol.* 9, 2019–2027.
- Na, X., Zang, S., Wang, J., 2009. Evaluation of random forest ensemble classification for land cover mapping using TM and ancillary geographical data. In: 2009 Sixth International Conference on Fuzzy Systems and Knowledge Discovery. IEEE, pp. 89–93.
- National Forest Inventory, 1998. Australia's State of the Forest Report 1998. In: Canberra.
- Nguyen, L.H., Henebry, G.M., 2019. Characterizing land use/land cover using multi-sensor time series from the perspective of land surface phenology. *Remote Sens.* 11, 1677.
- Olofsson, P., Foody, G.M., Stehman, S.V., Woodcock, C.E., 2013. Making better use of accuracy data in land change studies: estimating accuracy and area and quantifying uncertainty using stratified estimation. *Remote Sens. Environ.* 129, 122–131.
- Olofsson, P., Foody, G.M., Herold, M., Stehman, S.V., Woodcock, C.E., Wulder, M.A., 2014. Good practices for estimating area and assessing accuracy of land change. *Remote Sens. Environ.* 148, 42–57.
- Olson, D.M., Dinerstein, E., Wikramanayake, E.D., Burgess, N.D., Powell, G.V., Underwood, E.C., D'amico, J.A., Itoua, I., Strand, H.E., Morrison, J.C., 2001. Terrestrial Ecoregions of the world: a new map of life on EarthA new global map of terrestrial ecoregions provides an innovative tool for conserving biodiversity. *BioScience* 51, 933–938.
- Pelletier, C., Valero, S., Inglada, J., Champion, N., Marais Sicre, C., Dedieu, G., 2017. Effect of training class label noise on classification performances for land cover mapping with satellite image time series. *Remote Sens.* 9, 173.
- Penuelas, J., Filella, I., Biel, C., Serrano, L., Save, R., 1993. The reflectance at the 950–970 nm region as an indicator of plant water status. *Int. J. Remote Sens.* 14, 1887–1905.
- Peters, M.K., Hemp, A., Appelhans, T., Becker, J.N., Behler, C., Classen, A., Detsch, F., Ensslin, A., Ferger, S.W., Frederiksen, S.B., Gebert, F., Gerschlauer, F., Gütlein, A., Helbig-Bonitz, M., Hemp, C., Kindeketa, W.J., Kühnel, A., Mayr, A.V., Mwamgomo, E., Ngereza, C., Njovu, H.K., Otte, I., Pabst, H., Renner, M., Röder, J., Rutten, G., Schellenberger Costa, D., Sierra-Cornejo, N., Vollstädt, M.G.R., Dulle, H. I., Eardley, C.D., Howell, K.M., Keller, A., Peters, R.S., Ssymank, A., Kakengi, V., Zhang, J., Bogner, C., Böhning-Gaese, K., Brandl, R., Hertel, D., Huwe, B., Kiese, R., Kleyer, M., Kuzyakov, Y., Nauss, T., Schleuning, M., Tschapka, M., Fischer, M., Steffan-Dewenter, I., 2019. Climate-land-use interactions shape tropical mountain biodiversity and ecosystem functions. *Nature* 568, 88–92.
- Pontius Jr., R.G., Li, X., 2010. Land transition estimates from erroneous maps. *J. Land Use Sci.* 5, 31–44.
- Popp, A., Calvin, K., Fujimori, S., Havlik, P., Humpenöder, F., Stehfest, E., Bodirsky, B.L., Dietrich, J.P., Doelmann, J.C., Gusti, M., Hasegawa, T., Kyle, P., Obersteiner, M., Tabeau, A., Takahashi, K., Valin, H., Waldhoff, S., Weindl, I., Wise, M., Kriegler, E., Lotze-Campen, H., Fricko, O., Riahi, K., Vuuren, D.P.v., 2017. Land-use futures in the shared socio-economic pathways. *Glob. Environ. Chang.* 42, 331–345.
- Potere, D., Schneider, A., 2007. A critical look at representations of urban areas in global maps. *GeoJournal* 69, 55–80.
- Prestele, R., Alexander, P., Rounsevell, M.D., Arneth, A., Calvin, K., Doelman, J., Eitelberg, D.A., Engstrom, K., Fujimori, S., Hasegawa, T., Havlik, P., Humpenoder, F., Jain, A.K., Krisztin, T., Kyle, P., Meiyappan, P., Popp, A., Sands, R. D., Schaldach, R., Schungel, J., Stehfest, E., Tabeau, A., Van Meijl, H., Van Vliet, J., Verburg, P.H., 2016. Hotspots of uncertainty in land-use and land-cover change projections: a global-scale model comparison. *Glob. Chang. Biol.* 22, 3967–3983.
- Qi, J., Chehbouni, A., Huete, A., Kerr, Y., Sorooshian, S., 1994. A modified soil adjusted vegetation index. *Remote Sens. Environ.* 48, 119–126.
- Reichstein, M., Camps-Valls, G., Stevens, B., Jung, M., Denzler, J., Carvalhais, N., Prabhat, 2019. Deep learning and process understanding for data-driven earth system science. *Nature* 566, 195–204.
- Rodriguez-Galiano, V.F., Ghimire, B., Rogan, J., Chica-Olmo, M., Rigol-Sánchez, J.P., 2012. An assessment of the effectiveness of a random forest classifier for land-cover classification. *ISPRS J. Photogramm. Remote Sens.* 67, 93–104.
- Rondeaux, G., Steven, M., Baret, F., 1996. Optimization of soil-adjusted vegetation indices. *Remote Sens. Environ.* 55, 95–107.
- Roodposhti, M.S., Aryal, J., Bryan, B.A., 2019. A novel algorithm for calculating transition potential in cellular automata models of land-use/cover change. *Environ. Model. Softw.* 112, 70–81.
- Scarth, P., Armston, J., Flood, N., Denham, R., Collett, L., Watson, F., Trevithick, B., Muir, J., Goodwin, N., Tindall, D., 2015. Operational application of the landsat timeseries to address large area landcover understanding. *Int. Arch. Photogramm. Remote. Sens. Spat. Inf. Sci.* 40, 571.
- Scarth, P., Armston, J., Lucas, R., Bunting, P., 2019. A structural classification of Australian vegetation using ICESat/GLAS, ALOS PALSAR, and Landsat sensor data. *Remote Sens.* 11, 147.
- Seabrook, L., McAlpine, C., Fensham, R., 2006. Cattle, crops and clearing: regional drivers of landscape change in the Brigalow Belt, Queensland, Australia, 1840–2004. *Landsc. Urban Plan.* 78, 373–385.
- Seto, K.C., Fragkias, M., Güneralp, B., Reilly, M.K., 2011. A meta-analysis of global urban land expansion. *PLoS One* 6, e23777.
- Shadman Roodposhti, M., Aryal, J., Lucieer, A., Bryan, B.A., 2019a. Uncertainty assessment of hyperspectral image classification: deep learning vs. random forest. *Entropy* 21, 78.
- Shadman Roodposhti, M., Lucieer, A., Anees, A., Bryan, B.A., 2019b. A robust rule-based ensemble framework using mean-shift segmentation for Hyperspectral image classification. *Remote Sens.* 11, 2057.
- Shannon, C.E., 1948. A mathematical theory of communication. *Bell Syst. Tech. J.* 27, 379–423.
- Simmons, B.A., Law, E.A., Marcos-Martinez, R., Bryan, B.A., McAlpine, C., Wilson, K.A., 2018a. Spatial and temporal patterns of land clearing during policy change. *Land Use Policy* 75, 399–410.
- Simmons, B.A., Marcos-Martinez, R., Law, E.A., Bryan, B.A., Wilson, K.A., 2018b. Frequent policy uncertainty can negate the benefits of forest conservation policy. *Environ. Sci. Pol.* 89, 401–411.
- Simmons, B.A., Wilson, K.A., Marcos-Martinez, R., Bryan, B.A., Holland, O., Law, E.A., 2018c. Effectiveness of regulatory policy in curbing deforestation in a biodiversity hotspot. *Environ. Res. Lett.* 13, 124003.
- Song, X.-P., Hansen, M.C., Stehman, S.V., Potapov, P.V., Tyukavina, A., Vermote, E.F., Townshend, J.R., 2018. Global land change from 1982 to 2016. *Nature* 560, 639–643.
- South Australian Department for Environment and Water, 2018. SA Land Cover. South Australian Department for Environment and Water.
- Tan, P., Lymburner, L., Mueller, N., Li, F., Thankappan, M., Lewis, A., Ieee, 2013. Applying machine learning methods and time series analysis to create a national dynamic land cover dataset for Australia. In: 2013 IEEE International Geoscience and Remote Sensing Symposium, pp. 4289–4292.
- Team, R.C., 2013. R: A Language and Environment for Statistical Computing.
- Teluguntla, P., Thenkabail, P.S., Oliphant, A., Xiong, J., Gumma, M.K., Congalton, R.G., Yadav, K., Huete, A., 2018. A 30-m landsat-derived cropland extent product of Australia and China using random forest machine learning algorithm on Google earth engine cloud computing platform. *ISPRS J. Photogramm. Remote Sens.* 144, 325–340.
- Thackway, R., Cresswell, I.D., 1995. An Interim Biogeographic Regionalisation for Australia: A Framework for Setting Priorities in the National Reserves System Cooperative. Australian Nature Conservation Agency, Reserve Systems Unit.
- Townshend, J.R., Masek, J.G., Huang, C., Vermote, E.F., Gao, F., Channan, S., Sexton, J. O., Feng, M., Narasimhan, R., Kim, D., Song, K., Song, D., Song, X.-P., Noojipady, P., Tan, B., Hansen, M.C., Li, M., Wolfe, R.E., 2012. Global characterization and monitoring of forest cover using Landsat data: opportunities and challenges. *Int. J. Digital Earth* 5, 373–397.
- Turner, B.L., Lambin, E.F., Reenberg, A., 2007. The emergence of land change science for global environmental change and sustainability. *Proc. Natl. Acad. Sci.* 104, 20666–20671.
- van Vliet, J., Bregt, A.K., Brown, D.G., van Delden, H., Heckbert, S., Verburg, P.H., 2016. A review of current calibration and validation practices in land-change modeling. *Environ. Model. Softw.* 82, 174–182.
- Verburg, P.H., Schot, P.P., Dijst, M.J., Veldkamp, A., 2004. Land use change modelling: current practice and research priorities. *GeoJournal* 61, 309–324.
- Verburg, P.H., Crossman, N., Ellis, E.C., Heinemann, A., Hostert, P., Mertz, O., Nagendra, H., Sikor, T., Erb, K.-H., Golubiewski, N., Grau, R., Grove, M., Konaté, S., Meyfroidt, P., Parker, D.C., Chowdhury, R.R., Shibata, H., Thomson, A., Zhen, L., 2015. Land system science and sustainable development of the earth system: a global land project perspective. *Anthropocene* 12, 29–41.
- Vidal-Macua, J.J., Zabala, A., Ninyerola, M., Pons, X., 2017. Developing spatially and thematically detailed backdated maps for land cover studies. *Int. J. Digital Earth* 10, 175–206.
- Wang, S., Azzari, G., Lobell, D.B., 2019. Crop type mapping without field-level labels: random forest transfer and unsupervised clustering techniques. *Remote Sens. Environ.* 222, 303–317.
- Wold, S., Esbensen, K., Geladi, P., 1987. Principal component analysis. *Chemom. Intell. Lab. Syst.* 2, 37–52.
- Wulder, M.A., White, J.C., Goward, S.N., Masek, J.G., Irons, J.R., Herold, M., Cohen, W. B., Loveland, T.R., Woodcock, C.E., 2008. Landsat continuity: issues and opportunities for land cover monitoring. *Remote Sens. Environ.* 112, 955–969.
- Xiong, J., Thenkabail, P., Tilton, J., Gumma, M., Teluguntla, P., Oliphant, A., Congalton, R., Yadav, K., Gorelick, N., 2017. Nominal 30-m cropland extent map of continental Africa by integrating pixel-based and object-based algorithms using Sentinel-2 and Landsat-8 data on Google earth engine. *Remote Sens.* 9, 1065.
- Young, N.E., Anderson, R.S., Chignell, S.M., Vorster, A.G., Lawrence, R., Evangelista, P. H., 2017. A survival guide to Landsat preprocessing. *Ecology* 98, 920–932.
- Zha, Y., Gao, J., Ni, S., 2003. Use of normalized difference built-up index in automatically mapping urban areas from TM imagery. *Int. J. Remote Sens.* 24, 583–594.
- Zhang, Q., Li, B., Thau, D., Moore, R., 2015. Building a better urban picture: combining day and night remote sensing imagery. *Remote Sens.* 7, 11887–11913.
- Zhu, Z., Gallant, A.L., Woodcock, C.E., Pengra, B., Olofsson, P., Loveland, T.R., Jin, S., Dahal, D., Yang, L., Auch, R.F., 2016. Optimizing selection of training and auxiliary data for operational land cover classification for the LCMAP initiative. *ISPRS J. Photogramm. Remote Sens.* 122, 206–221.